Kato, A. S., Burris, K. D., Gardinier, K. M., Gernert, D. L., Porter, W. J., Reel, J., Ding, C., Tu, Y., Schober, D. A., Lee, M. R., Heinz, B. A., Fitch, T. E., Gleason, S. D., Catlow, J. T., Yu, H., Fitzjohn, S. M., Pasqui, F., Wang, H., Qian, Y., ... Witkin, J. M. (2016). Forebrain-selective AMPA-receptor antagonism guided by TARPλ 3-8 as an antiepileptic mechanism. *Nature Medicine*, *22*(12), 1496-1501. https://doi.org/10.1038/nm.4221

Peer reviewed version

License (if available):
Unspecified

Link to published version (if available):
10.1038/nm.4221

Forebrain-selective AMPA-receptor antagonist guided by TARP γ-8 as a novel antiepileptic

Akihiko S Kato[1], Kevin D Burris[1], Kevin M Gardinier[1], Douglas L Gernert[1], Warren J. Porter[1], Jon Reel[1], Chunjin Ding[1], Yuan Tu[1], Douglas A Schober[1], Matthew R Lee[2], Beverly A Heinz[1], Thomas E Fitch[1], Scott D Gleason[1], John T Catlow[1], Hong Yu[1a], Stephen M. Fitzjohn[3b], Francesca Pasqui[3], He Wang[1], Yuewei Qian[1], Emanuele Sher[3], Ruud Zwart[3], Keith A. Wafford[3,] Kurt Rasmussen[1], Paul L Ornstein[1c], John TR Isaac[3d], Eric S Nisenbaum[1], David S Bredt[1a], and Jeffrey M Witkin[1]

[1] Lilly Research Laboratory, Eli Lilly and Company, Indianapolis, IN 46285, USA

[2]Applied Molecular Evolution, Eli Lilly and Company, San Diego, CA 92121, USA

[3] Lilly UK, Eli Lilly and Company, Windlesham, Surrey, GU20 6PH, UK

a, Present address: Janssen PRD, San Diego, CA

b, Present address: School of Physiology, Pharmacology and Neuroscience, University of Bristol, Bristol, UK

c, Present address: College of Pharmacy, Roosevelt University, Schaumburg, IL

d, Present address: Wellcome Trust, London UK

Corresponding authors: Akihiko S. Kato or Jeffrey M. Witkin,

E-Mail: katoak@lilly.com or jwitkin@lilly.com

Pharmacological manipulation of specific neural circuits to optimize the therapeutic index is an unrealized goal in neurology and psychiatry. AMPA receptors play key roles in excitatory synaptic transmission [1], and their antagonists are antiepileptic [2]. Although efficacious, AMPA receptor antagonists, including perampanel (Fycompa), the only approved antagonist for epilepsy, induce dizziness and motor impairment [3,4]. We hypothesized that blockade of forebrain AMPA receptors that spared the cerebellum would be antiepileptic and devoid of motor impairment. Taking advantage of an AMPA receptor auxiliary protein, TARP γ-8, which is selectively expressed in the forebrain and modulates the pharmacological properties of AMPA receptors [5], we discovered LY3130481 that selectively antagonized recombinant and native AMPA receptors containing γ-8-but not γ-2 (cerebellum) or other TARP members. Two amino acid residues unique to γ-8 determine this selectivity. Antagonism was also observed in AMPA receptors expressed in hippocampal tissue from an epileptic patient but not in tissue from cerebellum. Corresponding to this selective activity, LY3130481 prevented multiple seizure types in rodents and was devoid of motor side-effects. These findings demonstrate the first rationally-discovered molecule targeting specific neural circuitries for therapeutic advantage.

Perampanel (Fycompa) [2], used to control refractory partial seizures, blocks cerebellar AMPA receptors with similar potency and efficacy to hippocampal receptors and induces sedation and ataxia in rodents and dizziness and falling in patients [3,4] We developed a high-throughput intracellular calcium dye-based assay, FLIPR, to identify compounds that specifically block AMPA receptors associated with TARP γ-8. Glutamate stimulated an increase in calcium flux in CHO-S cells transfected with GluA1-Flip (GluA1i) alone or co-transfected with GluA1-Flop (GluA1o) and either γ-2 or γ-8. Co-application of glutamate with cyclothiazide (CTZ), an AMPA receptor potentiator, enhanced the response (Fig. 1a), consistent with established electrophysiological data [5,6]. Detection of large kainate-evoked responses in cells expressing GluA1o + γ-2- or GluA1o + γ-8, but not in cells expressing GluA1i alone (Fig. 1b), is consistent with increased kainate efficacy in the presence of TARPs [7,8]. GYKI53784, which completely blocks AMPA receptor-mediated currents, also blocked calcium influx in all transfections (Fig. 1c).

We then screened several thousand compounds from the Lilly collection for their ability to block glutamate/CTZ-stimulated calcium responses in cells expressing GluA1o+ γ-8. Active compounds were examined in cells expressing GluA1i alone and in cells expressing GluA1o + γ-2 to identify TARP-dependent and TARP subtype-selective activity, respectively. Subsequent chemical structure-activity relationship (SAR) studies led to the discovery of LY3130481 (6-((*S*)-1-{1-[5-(2-hydroxy-ethoxy)-pyridin-2-yl]-1H-pyrazol-3-yl}-ethyl)-3- H-1,3-benzothiazol-2-one), which potently blocked GluA1o + γ-8, but not GluA1i alone or GluA1o + γ-2 (Fig. 1d, e, g). Detailed chemical synthesis and the SAR of LY3130481 were described elsewhere [9]. LY3130481 is not related to any known category or class of compounds in clinical use. As previously published [10], GYKI53784 inhibited GluA1 receptors without preference for γ-2 vs. γ-8 (Fig. 1f).

We further explored the pharmacology of LY3130481 by voltage clamp recordings. Glutamate application on GluA1i-transfected cells evoked inward currents, which rapidly desensitized to a small steady-state current, and TARP co-transfection dramatically modified these characteristics (Supplementary Fig. 1) [5,11]. LY3130481 potently and efficaciously blocked glutamate-evoked currents in cells transfected with GluA1i + γ-8 (Fig. 2a). LY3130481 had minimal effect on the other recombinant channels with the exception of GluA1i + γ-4 (the closest γ-8 homologue) [5], for which it displayed ~100-fold lower potency. LY3130481 also had no effect on GluA1i alone or GluA1i + CNIH-2 (another AMPA receptor associated protein) [12,13] or + γ-5 (Fig. 2a, Supplementary Fig. 1, Supplementary Table 1a). Perampanel blocked AMPA receptors independent of TARPs, as did GYKI53784 (Supplementary Fig. 2, Supplementary Table 1b, 1c). LY3130481 potently and efficaciously blocked all γ-8-containing

homomeric AMPA receptors that display measurable steady-state glutamate evoked currents (GluA1i, GluA2i, GluA3i, GluA4i and GluA1o) indicating that the γ-8-specific antagonistic actions were not GluA subunit-dependent (Fig. 2a-2e, Supplementary Fig. 3, Supplementary Table 1a). GluA2o, GluA3o, GluA4o homomers did not show measurable currents. LY3130481 also antagonized γ-8 containing GluA1/2 heteromers, the primary AMPA receptor in hippocampal neurons [14]. CNIH-2/3 play a critical role in native hippocampal AMPA receptors [15] and LY3130481 potently blocked GluA1/2 heteromers containing γ-8 + CNIH-2, whereas it only minimally antagonized CNIH-2-containing AMPA receptors with either γ-2 or γ-4 (Fig. 2f, Supplementary Fig. 4, Supplementary Table 1a). Since CNIH-2 reduces γ-8 stoichiometry of AMPA receptors [16], we wondered whether the partial inhibition was explained by fewer γ-8 molecules per AMPA receptor. We therefore trimmed γ-8 stoichiometry using a GluA1i/γ-8 tandem construct co-transfected with GluA1i or GluA2i [13,16]. Indeed, LY3130481 was less efficacious and slightly less potent against AMPA receptors with lower γ-8 stoichiometry (Fig. 2g, Supplementary Fig. 4a-f, Supplementary Table 1a). LY3130481 antagonized GluA2i + γ-8 less efficaciously than the other γ-8 containing AMPA receptors (Fig. 2b). This difference is not likely due to low γ-8 stoichiometry to GluA2i, but the intrinsic properties of GluA2i + γ-8 with high-γ-8 stoichiometry (Supplemental Fig. 4a, 4g-i). Hill coefficients (nH) for LY3130481 antagonism showed no strong cooperativity in either γ-8 containing AMPA receptors (Supplementary Table 1a). Glutamate concentration response curves revealed that LY3130481 displayed non-competitive antagonist characteristics (Fig. 2h, Supplementary Table 1d).

Domain swapping and mutational studies between γ-8 and γ-4 revealed that two amino acids (valine 177 and glycine 210 in transmembrane domains 3 and 4, respectively) close to the extracellular milieu were critical for the selectivity of LY3130481 (Fig. 2i, Supplementary Fig. 5-7, Supplementary Table 1e). Since these two amino acids are unique to γ-8 and not present in other Type I TARPs (Supplementary Fig. 6f), we generated the corresponding γ-2 point mutants. Consistent with the γ-4 mutants, double amino-acid substitution in γ-2 conferred high sensitivity to LY3130481 and the single amino-acid substitutions yielded moderate sensitivity to LY3130481 (Fig. 2k, Supplementary Fig. 8, Supplementary Table 1e).

LY3130481 antagonized AMPA receptors in hippocampal or cerebrocortical neurons, but not cerebellar Purkinje neurons (Fig. 3a, Supplementary Fig. 9a, Supplementary Table 1f). The partial inhibition profile of LY3130481 in neurons was comparable to that observed in recombinant AMPA receptors with reduced γ-8 stoichiometry, i.e. CNIH-2 containing or GluA1i/γ-8 tandem + GluA (Fig. 2f, 2g, Supplementary Table 1a). Crucially, LY3130481 was not active on hippocampal neurons from γ-8$^{-/-}$ mice

(Fig. 3b, Supplementary Fig. 9b). In contrast, perampanel did not show brain region specificity for AMPA receptor inhibition (Supplementary Fig. 9c, Supplementary Table 1f) [4].

LY3130481 also antagonized excitatory synaptic transmission. In rodent hippocampal slices, LY3130481 gradually and significantly blocked field excitatory postsynaptic potential (fEPSP) at Schaffer collateral – CA1 synapses (Fig. 3c-3f), whereas it was inactive in γ-8$^{-/-}$ mice (Fig. 3c, 3d). The slow onset of fEPSP blockage by LY3130481 in hippocampal slices (Fig. 3d,e) is likely due to slow LY3130481 penetration into the slices (Supplementary Fig. 10). Selectivity analyses of LY3130481 to other receptors, ion channels and transporters revealed that LY3130481 did not exhibit significant (>40%) modulation of radioligand binding (Supplementary Table 2), and FLIPR assays revealed that LY3130481 did not functionally modulate any of kainate, NMDA or metabotropic glutamate receptors (Supplementary Table 3a, 3b). To assess LY3130481 effects *in vivo*, we counted the spikes evoked by either iontophoretically-applied AMPA or NMDA in CA1 hippocampal regions of anesthetized rats. Both AMPA and NMDA evoked robust and transient spikes. Systemically-administered LY3130481 reduced AMPA-evoked, but not NMDA-evoked activities in a dose dependent manner (Fig. 3g, h). Critically, AMPA-evoked spiking activity was not antagonized in the rat red nucleus, a brain area, like cerebellum, with very low density of TARP γ-8 (Supplementary Figure 10). The molecular mechanisms underlying the blockage of γ-8-contatning AMPA receptors by LY3130481 is not clear. Pharmacological and biochemical analyses suggest that LY3130481 does not likely involve dissociation of γ-8 from AMPA receptors (Supplementary Fig. 12)

Oral administration of LY3130481 potently and dose-dependently suppressed the clonic convulsions induced by pentylenetrazole (PTZ) in rats (ED_{50}=1.7 mg/kg) (Fig. 4a). No motor deficits were observed up to 100 mg/kg (Fig. 4b**).** In contrast, GYKI52466 and perampanel were anticonvulsant (Fig. 4a) only at a dose that produced profound motor impairment (Fig. 4b). LY3130481 and perampanel also functioned as an anticonvulsant in rodents fully sensitized to repeated daily exposure to electrically-induced seizures (kindling) via the basolateral amygdala (Fig. 4c), without any noted motoric changes after LY3130481 dosing in the epileptic animals. Notably, and in contrast to perampanel, LY3130481 produced small increases in locomotion, fitting γ-8$^{-/-}$ mice showing hyper-locomotor activities [17] (Fig 4d). The anticonvulsant effects of LY3130481 were abolished in γ-8$^{-/-}$ mice, whereas the anticonvulsant effects of GYKI52466 and perampanel remained (Fig. 4e). Perampanel (1 and 2 mg/kg) induced tremor, ataxia, running, bouncing, and tonic-clonic forelimb seizures with falling in mice with kainate-induce mesial temporal lobe epilepsy, effects not observed in non-epileptic mice [18]. Therefore, we conducted two experiments to evaluate effects of LY3130481 in epileptic mice. Mice with kainate-induced mesial

temporal lobe epilepsy exhibited 16.3 $\pm$ 1.3 spontaneous recurrent hippocampal paroxysmal discharges and these were completely eliminated 15 minutes following treatment with LY3130481 (6 mg/kg, i.p). In mice kindled with PTZ (45 mg/kg, s.c., every other day) for 5 days, the percentage of mice exhibiting clonus was 83.0 $\pm$ 7.3 (n=24) on day 8. Both LY3130481 (10 mg/kg, i.p.) and perampanel (30 mg/kg, i.p.) significantly reduced kindled seizures (Fig 4f). However, perampanel but not LY3130481 engendered motor impairment in naïve and PTZ-kindled mice (Fig 4f, insert). LY3130481 also engendered a qualitatively different motor signature in mice than perampanel, with increases in ambulations and vertical movements, whereas, perampanel decreased these behaviors (Fig.4g). . We next reconstituted AMPA receptors from hippocampal tissue obtained from an epileptic patient into *Xenopus* oocytes [4]. These AMPA receptor currents were dose-dependently attenuated by LY3130481 (Fig. 4h, i), whereas comparable AMPA currents from the human cerebellum were not (Fig 4j). Perampanel blocked AMPA currents in both cortex and cerebellum {Zwart, 2014 #2859}.

This work illustrates the engineering of a selective modulator of forebrain function based on a specific auxiliary protein for a receptor regulating fast synaptic transmission Although there are marketed drugs that interact with auxiliary subunits of other ion channels (e.g. gabapentin for the $\alpha 2\delta$ subunit of voltage-gated calcium channels and sulfonylurea drugs for the SUR subunit of K_{ATP} channels), neither the drugs nor their mechanisms of action were rationally designed nor directed towards regional circuits. Recent studies show that several neurotransmitter receptors contain auxiliary subunits [5,19]. Systematic screening of compounds that selectively target auxiliary proteins as described here will enable identification of chemicals that selectively modulate brain areas involved in disease while minimizing side-effects. Since neuronal receptors can associate with a range of auxiliary proteins that have differential localization and functional controls over specific neural circuits, the current strategy has far-reaching consequences.

Main Figure legends

Figure 1. Identification of γ-8-selective AMPA receptor antagonists. a-d. Representative time-courses of $[Ca^{2+}]_i$ measurements in Fluo-4-AM loaded CHO-S cells transfected with GluA1i alone, GluA1o + γ-2, or GluA1o + γ-8 by using the FLIPR multi-well calcium measurement system (See Methods section). Bars below the graphs indicate the timing of compound application. Final compound concentrations: Glutamate (5 μM) and then glutamate (45 μM) + CTZ (20 μM); Kainate (15 μM); GYKI (167 μM); LY3130481 (9.3 μM). FU, Fluorescence unit. **(e)** The chemical structure of LY3130481, 6-((*S*)-1-{1-[5-(2-hydroxy-ethoxy)-pyridin-2-yl]-1H-pyrazol-3-yl}-ethyl)-3- H-1,3-benzothiazol-2-one. [US patent 8,765,960]. **(f-g)** Concentration-response curves for GYKI53784 **(f)** and LY3130481 **(g)** against the glutamate + CTZ responses. Figures 1f and g are shown as individual experiments for which replications exist (GYKI: GluA1i, n = 275 assays; GluA1o + γ-8, n=157; GluA1o + γ-2 = 274); (LY3130481: GluA1i, n=26; GluA1o + γ-8, n=30; GluA1o + γ-2 = 28).

Figure 2. LY3130481 potently and selectively blocked all AMPA receptor complexes that contain γ-8. **(a-e)** Concentration-response curves (CRCs) for inhibition of glutamate-evoked currents by LY3130481 in HEK293T cells transfected with GluA1i **(a)**, GluA2i **(b)**, GluA3i **(c)**, GluA4i **(d)**, GluA1o **(e),** GluA1i + GluA2i heteromers **(f)** and auxiliary subunits as indicated. Responses were evoked by 1 mM glutamate and steady-state currents measured. **(g)** The CRCs of LY3130481 for the AMPA receptors with stoichiometric manipulations using the co-expression of GluA1i or GluA2i with GluA1i/γ-8 tandem. The major recombinant AMPA receptors with GluA1i + γ-8 or GluA1i/γ-8 tandem alone have higher γ-8 stoichiometry than those formed with CNIH-2 + GluA1i + γ-8 or GluA + GluA1i/γ-8 tandem [13,16]. **(h)** Non-competitive antagonism by LY3130481 Relative amplitude of steady-state currents evoked by glutamate is plotted as the function of glutamate concentration in the presence of LY3130481 at various concentrations. Data points and error bars are mean ± SEM. The number of the recorded transfectants and IC_{50} are in Supplemental Table 1a and 1d **(i, j)** Identification of two amino acids crucial for the selectivity of LY3130481 IC_{50} of LY3130481 for the glutamate-evoked currents through GluA1i + γ-8 **(i)** or γ-4 **(j)** point mutants are shown as bar graphs. We performed domain swapping between γ-8 and γ-4 and then identified the unique amino-acids for γ-8 shown in Supplementary Fig. 5-7. The number of the recorded transfectants and IC_{50} are in Supplemental Table 1e. Error bars indicate SEM. *; $p<0.001$ compared to GluA1 + γ-8, #; $p<0.001$ compared to GluA1 + γ-4 with Dunnett's test. (k) The potency of

LY3130481 in the γ-2 mutants substituted with γ-8 amino acids at the corresponding positions responsible for LY3130481 selectivity. *; p<0.001 compared to GluA1 + γ-2(I153V/A184G), #; p<0.001 compared to GluA1 + γ-2 with Dunnett's test.

Figure 3. LY3130481 potently and partially blocked native γ-8-containing, but not γ-8-lacking AMPA receptors. **(a)** CRCs for the inhibition of glutamate (1 mM)-evoked currents by LY3130481 on acutely-isolated rat hippocampal, cortical, and cerebellar Purkinje neurons. *; p<0.001 compared to the cerebellar neurons with Tukey's test **(b)** The CRCs of LY3130481 on acutely-isolated the hippocampal and cortical neurons from γ-$8^{+/+}$ or γ-$8^{-/-}$ mice. Error bars indicate SEM. The number of the recorded transfectants and IC_{50} are in Supplemental Table 1f. *; p<0.001 compared to the hippocampal or cortical neurons from γ-$8^{-/-}$ with Tukey's test γ-8 dependent blockage of fEPSP at hippocampal Schaffer-CA1 synaptic transmissions by LY3130481 **(c)** Typical traces before (green) and after (orange) the application of LY3130481 Scale bars, 10 ms, 0.1 mV **(d)** Change in the slopes of the first fEPSP is plotted as a function of time. LY3130481 The number of recordings, γ-$8^{+/+}$: n = 4 γ-$8^{-/-}$: n = 3. The time constant of fEPSP slope change in γ-$8^{+/+}$ slices by LY3130481 was calculated by fitting with single-phase decay curve ($\tau_{1\,\mu M}$ = 40 min). Data points and error bars are mean ± SEM. **(e)** Concentration-dependent reductions in the fEPSP slopes of rat Schaffer-CA1 synapses at various concentrations of LY3130481. (The time constant of change in fEPSP slopes: $\tau_{0.3\,\mu M}$ = 30 min, $\tau_{1.0\,\mu M}$ = 17 min, $\tau_{3.0\,\mu M}$ = 54 min, $\tau_{10\,\mu M}$ = 22 min) Data points and error bars are mean ± SEM. Parentheses indicate the number of recorded slices. **(f)** CRC of the LY3130481 for the rat hippocampal neurotransmission (mean ± SEM) by LY3130481 demonstrating an IC_{50} of 87.5 nM. **(g)** The field potential recordings evoked by iontophoretically administered AMPA or NMDA at the CA1 area of anesthetized rats with systemic injection of LY3130481 at different doses The field potential and the firing rate (spike number / s) are shown with green traces and blue bar graphs, respectively. **(h)** Dose-dependence of LY3130481 onthe ratio of the AMPA- to NMDA-evoked firing rate Data points and error bars are mean ± SEM.The number of recordings, Veh: n = 8, 0.1: n = 5, 0.3: n = 7, 1.0: n = 7, 3.0 n = 6 **; p<0.001, *; p<0.05 compared to vehicle control with Dunnett's test.

Figure 4. Anticonvulsant effects of LY3130481, on motor performance and on excitatory currents from AMPA receptors expressed in human hippocampal epileptic tissue **(a)**. Percent animals with convulsions induced by pentylenetetrazole as a function of LY3130481doses orally administered. **(b)** Motor impairment score as a function of LY3130481 doses. Per: perampanel, LY: LY3130481, GYKI: GYKI52466 **(c)** Effects of LY3130481 against fully-expressed basolateral amygdala kindled seizures

induced by 400μA. F=21.4, p<0.0001, n=8/group. ED_{50}=16.4 (8.2-29) mg/kg. * p < 0.05, Fisher's exact test compared to vehicle control value. V: vehicle; Valpro: valproic acid (300 mg/kg, i.p.); * p < 0.05, Fisher's exact test, n=5/group. **(d)** Effects of LY3130481 on locomotor activity of rats in comparison with perampanel. *p< 0.05, ANOVA followed by post-hoc Dunnett's test. **(e)** Comparative effects of LY3130481 (10 mg/kg) in γ-$8^{-/-}$ and γ-$8^{+/+}$ mice against pentylenetetrazole (PTZ)-induced seizuresEffects of GYKI52466 (30 mg/kg, i.p.) and perampanel (30 mg/kg, i.p.). * p<0.05, Fisher's exact probability test compared to PTZ alone **(f)** Seizure and motor ratings (inset) in the presence or absence of LY3130481 (10 mg/kg, i.p.) or perampanel (30 mg/kg, i.p.) for the mice that were seizure kindled by every other day dosing with PTZ. * p<0.05, Fisher's exact probability test compared to control (V). **(g)** Effects of LY3130481 vs. perampanel on locomotion of mice assessed by distance traveled (upper panel) and instances of vertically-directed behaviors such as rearing (lower panel) * p<0.05, ANOVA followed by post-hoc Dunnett's test compared to vehicle control (V). **(h)** Representative trace of currents evoked by AMPA + cyclothiazide through Xenopus oocyte membranes micro-implanted with human epileptic hippocampal tissue. LY3130481 (10 μM) was co-applied 5 min after the application of AMPA (100 μM) + cyclothiazide (30 μM). Scale bars, 5 min and 50 nA. . **(i).** The relative amplitude of steady-state AMPA + CTZ evoked currents in the presence of LY3130481 recorded from Xenopus oocyte with human hippocampal membrane fraction was plotted as a function of LY3130481. Data are means ± SEM of three independent experiments. IC_{50}: 114 nM. **(j)** The trace from the same experimental procedures except using human cerebellar membranes for micro-implantation Scale bars, 5 min and 20 nA

Acknowledgements

We are grateful to the NIH Anticonvulsant Screening Program of the U.S. National Institutes of Neurological Disorders and Stroke, National Institutes of Health (http://www.ninds.nih.gov/research/asp/) for their help with the mesial temporal lobe assessments. In particular, we are grateful for the expert support of Tracy Chen, Shamsi Raeissi, and program director John Kehne and to their associated laboratories at the University of Utah, directed by H. Steve White. We also thank Covance Laboratories, Greenfield, Indiana, in particular Deah Modlin, for their assistance with the amygdala kindling studies, and Matthew W Jeffries (Eli Lilly and Co.) for transfection. While this manuscript was under review, the following manuscripts were published: Gardinier et al., 2016 [9] describing the synthesis of LY3130481: Maher et al. 2016 [20] describing an alternative molecule with TARP γ-8 selectivity and anticonvulsant activity; Witkin and Gardinier, 2016 [21] describing that LY3130481 was the first TARP-dependent antagonist disclosed.

Author contributions

J.M.W. designed and interpreted the anticonvulsant and behavioral experiments, wrote the manuscript and served as the biological leader of the project. A.S.K. designed, performed and interpreted most of the electrophysiological / biochemical experiments and wrote the manuscript. K.D.B., C.D., Y.T., D.A.S and H.Y. designed, performed and interpreted the FLIPR screening experiments. K.M.G. (chemistry leader), D.L.G., W.J.P., J.R., B.A.H. and P.L.O. performed chemical design and synthesis of LY3130481. F.P. and S.M.F. contributed electrophysiological recordings from hippocampal slices. R.Z. and M.S. designed and performed the Xenopus oocyte experiment. Y.Q., H.W. and M.R.L designed and constructed the TARP mutant cDNAs. T.F. and K.R. designed and performed in-vivo electrophysiological recordings. S.D.G. and K. A. W. designed and conducted anticonvulsant and behavioral studies. J.T.C. planned and executed experiments on tissue permeability. J.T.R.I. and E.S.N. designed electrophysiological experiments and provided expert advice. D.S.B. initiated the project with the key concept of this study.

Competing financial interest

All authors were employees of Eli Lilly and Company. This work was supported by Eli Lilly and Company.

Online Methods

FLIPR screening Inhibition of glutamate-stimulated activation of AMPA receptors was determined in CHO-S cells (InVitrogen) that transiently express human GluA1 and TARPs. For GluA1-γ-8 transfection, we constructed the plasmids expressing human GluA1o and human γ-8 bi-cistronically using pBudCE4.1 vector (Thermo Fisher), and co-transfected it in CHO-S cells with human EAAT3 cDNA in a ratio of 2:3. For GluA1-γ-2 transfection of CHO-S cells, bi-cistronically expressing human GluA1o-and human γ-2 inserted in pBudCE4.1 (Thermo Fisher) was used. For the TARP-less AMPA receptors, we used human GluA1-flip (GluA1i) in pcDNA3.1 (Thermo Fisher). Due to the relatively small dynamic range of calcium dyes, we needed to make the FLIPR signals comparable between the AMPA receptors with and without TARPs. To solve the issue, we used Flip and Flop isoform for TARP-less and TARP-containing transfectants, respectively. Flip isoforms have greater conductance than Flop isoforms [22], and TARPs enhance AMPA receptor functions of both Flip and Flop isoforms [5]. Parental CHO-S cells were grown in suspension in 50/50 custom media to a density of $1x10^7$ cells/ml. 50/50 is a 1:1 (v/v) mixture of CD CHO (Gibco #10743) and a custom complete media. The custom complete media was made by adding 0.40 mg/L tropolone, 5.00 mg/L insulin, 20 mM HEPES, and 0.075% Pluronic® F68 to a custom basal media having the following formula: (values as mg/L unless otherwise specified) 11.01 anhydrous calcium chloride, 0.050 ferric nitrate-$9H_2O$, 0.420 ferrous sulfate-$7H_2O$, 28.64 anhydrous magnesium chloride, 48.84 anhydrous magnesium sulfate, 312.14 KCl, 5505.96 NaCl, 62.57 monobasic sodium phosphate, 71.28 anhydrous dibasic sodium phosphate, 0.432 zinc sulfate-$7H_2O$, 10.0 ethanolamine HCl, 6000 D-glucose (dextrose), 0.210 DL lipoic acid thioctic, 0.081 putrescine 2 HCl, 4.78 sodium hypoxanthine, 220.24 sodium pyruvate, 0.730 thymidine, 8.90 L-alanine, 211.23 L-arginine HCl, 15.02 L-asparagine H_2O, 13.31 L-aspartic acid, 62.67 cystine 2 HCl, 7.360 L-glutamic acid, 146.16 L-Glutamine, 30.0 glycine, 42.04 L-histidine HCl 2 H_2O, 105.11 L-isoleucine, 105.11 L-leucine, 146.16 L-lysine HCl, 30.03 L-methionine, 66.07 L-phenylalanine, 17.27 L-proline, 42.04 L-serine, 95.1 L-threonine, 16.02 L-tryptophan, 104.11 L-tyrosine disodium salt, 94.1 L-valine, 8.99 choline chloride, 4.00 folic acid, 12.61 inositol, 4.00 niacinamide, 4.00 pyridoxal HCl, 0.031 pyridoxine HCl, 0.400 riboflavin, 4.00 sodium pantothenate, 4.00 thiamine HCl, 0.680 vitamin B12, and 2200 sodium bicarbonate.) Cells were centrifuged at 1000 x g for 15 min. and resuspended in fresh 50/50 custom media at $2x10^6$ cells/ml. For batch transfection, 2 mg of total DNA(s) was used for each liter of cells. DNA(s) and FreeStyleMAX® (Thermo Fisher cat#16447-500)

were added to basal custom media (see above) in the proportions of 10 µg total DNA : 10 µl FreeStyleMAX® : 1 ml media, to form a DNA complex. After 15 min., an appropriate volume (20% v/v) of DNA complex was added to the prepared cell culture. Transiently transfected CHO-S cells were harvested after 48 hours and frozen in aliquots for later use. The function and pharmacology of AMPA receptors in transfected cells was verified in both freshly prepared and thawed aliquots of cells. Frozen transfected CHO-S cells expressing AMPA receptors were thawed and plated in Dulbecco's Modified Eagle Media (DMEM media) (Thermo Fisher, cat# 11960) containing 5% dialyzed Fetal Bovine Serum (Thermo Fisher, cat# 26400-036) and 20 mM HEPES at 50,000 cells per well in 384-well Poly-D-lysine coated plates (Becton Dickinson, cat#354663) and cultured overnight at 37°C. On the day of an experiment, two fluorescence dye loading buffers were prepared. Fluo-4-AM dye loading buffer consists of 5 µM Fluo-4 AM dye (Molecular Probes, cat# F-14202) in Hank's Balanced Salt Solution (HBSS) containing 20 mM HEPES (pH 7.4), 2.5 mM probenecid (Sigma, cat# P8761), and 5 nM Pluronic® F-127 (Molecular Probes, cat# P3000MP). Fluo-4 NW dye loading buffer was prepared by adding 100 ml of HBSS containing 20 mM HEPES (pH 7.4) and 2.5 mM probenecid to one bottle of Fluo-4 NW dye (Molecular Probes, high throughput pack, cat# F36205). Cultured GluA1-γ-8 and GluA1-γ-2 CHO-S cells were loaded with Fluo-4 AM dye loading buffer and incubated at 22°C for 2 hr. GluA1flip CHO-S cells were loaded with Fluo-4 NW dye loading buffer and incubated at 37°C for 30 min. followed by incubation for 90 min. at 22°C. Following incubations, the dye loading buffer in the cell plate was removed and fresh assay buffer was added. Assay buffer consisted of HBSS with 20 mM HEPES (pH 7.4), 2.5 mM probenecid and 4 mM $CaCl_2$. The assay was initiated by addition of compounds followed 2 minutes later by addition of glutamate (5 µM final concentration). Two minutes later, cyclothiazide (20 µM final concentration) and glutamate (45 µM final concentration) were added. Changes in intracellular [Ca^{2+}] were kinetically recorded by a fluorescence imaging plate reader (FLIPR). Inhibition of the effect of glutamate by test compounds was expressed as a percentage of the responses stimulated by glutamate plus CTZ in the presence of test compounds relative to the maximum inhibition defined by using 167 µM of GYKI53784, a non-selective AMPA antagonist, and the baseline defined by assay buffer alone. The actions of LY3130481 on kainate receptors were evaluated using the HEK293 cells (ATCC) stably expressing human GluK2Q. The Fluo-4-AM loaded cells were pre-incubated with 250 µg/ml concanavalin A for 30 min. To evaluate the antagonistic action of LY3130481, we added various concentration of LY3130481, and then added 100 µM glutamate. The effect of LY3130481 on NMDA receptors was tested using HEK293 cells with human GluN1 / GluN2A or GluN1 / GluN2B cDNA under the control of TET-on operator with CMV promotor. The expression of NMDA receptors were induced by

1 μg/ml doxycycline. To evaluate the potentiator action, we added various concentrations of LY3130481 and then 0.2 μM glutamate + 2.5 μM glycine. The antagonistic action was evaluated by addition of LY3130481 and then 2 μM glutamate + 2.5 μM glycine. To evaluate the effects of LY3130481 on metabotropic glutamate receptors, we used AV12 cells (ATCC) stably expressing either of mGluR1, 2, 3, 4, 5, or 8 with EAAT1. To translate the activation of Gi-coupled mGluRs, mGluR2, 3, 4 and 8, to calcium mobilization, we co-expressed with a promiscuous G-alpha protein, Gα15. The cells were loaded with a calcium indicator, Fluo-3-AM, Fluo-4-AM or Calcium-5 (Molecular Devices), and measured the change in the fluorescent intensity by the additions of 12.5-25 μM of LY3130481 and then glutamate. We used EC_{10} and EC_{90} concentrations of glutamate to evaluate potentiator and antagonist actions, respectively.

Chimeric cDNA Constructions The chimeric γ-8 and γ-4 constructs were engineered out by PCR. The junctions of the transmembrane and extracellular / intracellular domains were predicted by the report by Burgress [23] and our own sequence alignments. The regions of the designated domains are as follows (The number of amino acid residues). γ-8 (human Cacng8), TM1: 1-41, Ex1: 42-129, TM34: 158-228, C-term: 229-425, TM3: 158-179, Ex2: 180-205, TM4: 206-228. γ-4 (human Cacng4), TM1: 1-30, Ex1: 31-108, TM34: 137-207, C-term: 208-327, TM3: 137-158, Ex2: 159-184, TM4: 185-207. Point mutations were generated by PCR-based site directed mutagenesis using custom oligonucleotides and Quikchange II kit (Agilent Technologies). GluA1/γ-8 construct was described previously [16].

Patch Clamp Electrophysiology Agonist-evoked currents were recorded from transfected HEK293T cells (ATCC) and acutely isolated neurons as described [24]. The rat neurons were isolated from 4-10 weeks old Sprague Dawley rats. The mouse neurons were from 4-10 weeks old CD-1 mice (γ-$8^{+/+}$) or γ-$8^{-/-}$ mice [25] that were back-crossed multiple times with CD-1 mice. We used both male and female animals for these studies. Kainate / glutamate ratios were calculated as:

$$I_{KA\text{-}steady\text{-}state} / I_{Glu\text{-}steady\text{-}state},$$

where $I_{KA\text{-}steady\text{-}state}$ and $I_{Glu\text{-}steady\text{-}state}$ are the steady state responses evoked by kainate (1 mM) and glutamate (1 mM) application, respectively.

Resensitization percentage was calculated as:

$$I_{Glu\text{-}Resens} / I_{Glu\text{-}steady\text{-}state} \times 100,$$

where $I_{Glu\text{-}Resens}$ is the current that accrues from the trough of desensitization [15]. We discarded less than 5% of total recorded the recombinant samples, which did not meet the criteria described in Supplementary Fig. 1-4, which validate the expression of the designated AMPA receptors and auxiliary subunits. We used all recordings from native neurons with stable and measurable steady-state currents. The potency of LY3130481 is calculated as follows. The amplitude of $I_{Glu\ Steady\text{-}state}$ in the presence of LY3130481 normalized by that in the absence of LY3130481 was defined it as "Relative $I_{Glu\ Steady\text{-}state}$", and plotted it as a function of Log_{10}[LY3130481]. The average and SEM of Log_{10}IC50 and efficacy (Imax) are calculated using the pooled Relative $I_{Glu\ Steady\text{-}state}$ values recorded from 3-19 cells as indicated in Figure Legends using three- or four-parameter sigmoidal curve fit with Prism 6.04 (GraphPad Software Inc.). We perfused 5-6 different concentrations of LY3130481 onto each cell. We put zero-drug values, i.e. Relative $I_{Glu\ Steady\text{-}state}$ without LY3130481 (= 1), at [LY3130481] = 1 x 10^{-13} M, which is 3 log unit below the lowest LY3130481 concentration tested. We did not constrain either the bottom or top values for the curve fitting calculations, so the calculated IC50 is relative IC50, in which halfway between the top and bottom plateau. To obtain reliable Hill slopes, we calculated Hill coefficient (nH) when we measured more than 12 concentration points. The potency of glutamate is calculated as follows. We measure the $I_{Glu\ Steady\text{-}state}$ without LY3130481 first, and then measure it under the perfusion of a fixed concentration of LY3130481 indicated in Fig. 2g. The $I_{Glu\ Steady\text{-}state}$ in the presence of LY3130481 was normalized by the $I_{Glu\ Steady\text{-}state}$ evoked by the initial 1 mM glutamate application without LY 3130481, and plotted as the function of Log_{10}[Glu]. We used three-parameter sigmoidal curve fit and calculated the average and SEM of Log_{10}IC50 and Emax using the pooled values of Relative $I_{Glu\ Steady\text{-}state}$ recorded from 3 cells for each concentration of LY3130481. We tested 4 glutamate concentrations for each cells. We put zero-glutamate values, i.e. Relative $I_{Glu\ Steady\text{-}state}$ without glutamate (= 0), at [Glu] = 1 x 10^{-8} M, which is 2 log unit below the lowest glutamate concentration tested.

Field EPSP recordings Field EPSPs (fEPSPs) were recorded from Schaffer-CA1 synapses of rats or mice described above. Parasagittal brain slices (400 μm thick) were prepared from 3-6 weeks old animals using Vibroslice (Campden Instruments, London or Leica, Milton Keynes, UK) in carbogenated (95% O_2 and 5% CO_2) ice cold slicing solution (concentrations in mM): NaCl 124, $NaHCO_3$ 26, KCl 3, glucose 10, $CaCl_2$ 0.5, $MgCl_2$ 4 with 300-305 mOsm. The slices are incubated at 30–34°C in carbogenated recording solution: NaCl 124, $NaHCO_3$ 26, KCl 3, glucose 10, $CaCl_2$ 2.3, $MgCl_2$ 1.3 with 300-305 mOsm for 30 minutes, and then allowed to rest at room temperature for another 30 minutes before recording. Slices were then placed in a submersion type recording chamber (RC-26G, Warner Instruments) mounted on

an upright microscope (FN-1, Nikon) and continuously superfused (2-3 ml/minute) with carbogenated recording solution. A concentric tungsten stimulation electrode and a recording electrode filled with 2 M NaCl were placed at stratum radiatum. Test pulses (100 μs pulse width) were applied every 20 s (0.05 Hz) or 30 s (0.067 Hz). Stimulation intensity was determined to obtain 50~70% of the maximum responses that elicit population spikes. The fEPSP slope after continuous LY3130481 perfusion (28 min for 10 μM or 60 min for the other concentrations) was normalized by the baseline, the mean fEPSP slope 20 min prior to LY3130481 perfusion, and % depression was calculated. We used the data with stable baseline. Concentration effect functions were generated and enabled construction of a concentration/%depression function with mean ± SEM and the estimation of an IC_{50} value by three-parameter sigmoidal curve fitting methods within GraphPad Prism 6.04.

Iontophoretic application of AMPA and NMDA in rat hippocampus or red nucleus Male Sprague Dawley rats (250-350 g body weight) were anesthetized with 1.4 times body weight of 600 mg/mL urethane and implanted with a jugular cannula (PE 10 tubing attached to a 30-gauge needle) for intravenous (IV) drug administration. Subjects were administered solutions of either LY3130481 (0.1, 0.3 or 1 mg/kg), GYKI53784 or vehicle (20% Captisol), intravenously. Cannulated subjects were mounted on a rat stereotaxic frame, the skull was exposed, and a well opening was created, using a dental drill, at the following coordinates: AP -4.2, ML +2.4 for hippocampus, AP: -5.8 mm, ML: +0.8 – +1.1 mm for red nucleus. The dura was then cut, exposing the cortical surface. A 5-barrel micropipette assembly mounted onto a Narishige micro-drive was lowered to a depth of DV: 1.8 to 2.6 mm for hippocampus or DV: 6.4 to 7.8 mm for red nucleus. The pipette barrels were pre-filled with solutions as follows: Center recording barrel: 2 M NaCl; current balancing: 2 M NaCl; ejection vehicle: 190 mM NaCl, pH 8; AMPA: 1mM dissolved in the ejection vehicle; NMDA: 10 mM dissolved in the ejection vehicle. The pipette was slowly lowered to the target depth until a response from a CA1 pyramidal neuron or red nucleus neuron could be isolated and held. Signals were amplified by an XCell 3+ differential amplifier (Frederick Hauer Corporation). Low frequency cutoff was set to 1000 Hz, high frequency cutoff set to 2000 Hz and gain set to 20000. Recordings of the cells' firing activity were made using Spike2 software. Alternating Iontophoretic ejections of AMPA and NMDA were made using a Dagan 6400 Programmable Current Generator. Ejections currents were titrated until stable levels of responding to pulses of AMPA and NMDA could be established, and then were held fixed. A baseline recording was then made followed by recordings of the response to IV administration of eithervehicle, 0.1, 0.3 or 1 mg/kg of LY3130481. Data were analyzed using Spike2 software from CED. Cursor placement was used to demarcate AMPA and

NMDA ejection pulses, and these cursor regions were analyzed for spike frequency across baseline, and post-drug administration epochs. Ratios of AMPA to NMDA mean firing rates (MFR) were then computed and averaged for each 5-minute time interval post injection, and expressed as percent baseline for each drug dose. As variances of percent baseline AMPA to NMDA ratios are not equal as they approach 0, data were log transformed (Log10) for further statistical analysis. Statistical evaluation of compound-treatment effects were made by one-way ANOVA for repeated measures. Transformed values for each 5-minute effect mean, post injection, was treated as a repeated time measure. When significant p-values from ANOVA were revealed Dunnett's within-group dynamic multiple comparisons were evaluated to compare the effects of vehicle and drug dose treatments.

Microtransplantation of brain membrane to Xenopus Oocyte Membranes Frozen samples of human hippocampus and cerebellum were obtained from Oregon Brain Bank (Portland, Orego, U.S.A.) and Analytical Biological Services Inc. (Wilmington, Delaware, U.S.A.), respectively. The hippocampal sample was from a patient suffering from epilepsy, the cerebellar sample was from a control donor. Brain samples were kept frozen at -80°C and transport of the samples from the USA to the UK took place on dry ice. Membrane preparations from these tissues were prepared according to the method developed and described by [26-28]. In short: 0.1 – 0.5 g of tissue was homogenized in ice-cold glycine buffer (concentrations in mM: 200 glycine, 150 NaCl, 50 EGTA, 50 EDTA, 300 sucrose) to which 10 μl protease inhibitor cocktail (Sigma) was added per ml glycine buffer. The homogenate was centrifuged at 4°C for 15 min at 9500 g. The supernatant was subsequently centrifuged at 4°C for 2 hrs at 100,000 g with an ultra-centrifuge and the pellet was re-suspended in ice-cold assay buffer (5 mM glycine). The protein concentration of the membrane preparations were measured using the Pierce BCA protein assay kit (Thermo Scientific, Rockford, IL, U.S.A.) and were around 3 mg/ml. Aliquots of the suspensions were kept at -80°C and were thawed just before injection into *Xenopus* oocytes. *Xenopus* oocytes (stage V-VI) were removed from schedule I sacrificed frogs and defolliculated after treatment with collagenase type I (5 mg/ml calcium-free Barth's solution) for 4 h at room temperature. 60 nl of membrane suspension was injected per oocyte using a Drummond (Broomall, PA, U.S.A.) variable volume microinjector. After injection, oocytes were incubated at 18°C in a modified Barth's solution containing (concentrations in mM): NaCl 88, KCl 1, $NaHCO_3$ 2.4, $Ca(NO_3)_2$ 0.3, $CaCl_2$ 0.41, $MgSO_4$ 0.82 , HEPES 15 and 50 mg/l neomycin (pH 7.6 with NaOH; osmolarity 235 mOsm). Experiments were performed on oocytes after 2-5 days of incubation. Oocytes were placed in a recording chamber (internal diameter 3 mm), which was continuously perfused with a saline solution (concentrations in mM): NaCl 115, KCl 2.5, $CaCl_2$ 1.8, $MgCl_2$

1, HEPES 10, pH 7.3 with NaOH, 235 mOsm) at a rate of approximately 10 ml/min. Dilutions of drugs in external saline were prepared immediately before the experiments and applied by switching between control and drug-containing saline using a BPS-8 solution exchange system (ALA Scientific Inc., Westbury, NY, U.S.A.). Between responses oocytes were washed for 2 min. Oocytes were impaled by two microelectrodes filled with 3 M KCl (0.5 – 2.5 MΩ) and voltage-clamped using a Geneclamp 500B amplifier (Axon Instruments, Union City, CA, U.S.A.). The external saline was clamped at ground potential by means of a virtual ground circuit using an Ag/AgCl reference electrode and a Pt/Ir current-passing electrode. The membrane potential was held at -60 mV. The current needed to keep the oocyte's membrane at the holding potential was measured. Membrane currents were low-pass filtered (four-pole low-pass Bessel filter, -3 dB at 10 Hz), digitized (50 Hz), and stored on disc for offline computer analysis. Data are expressed as mean ± SEM. Experiments were performed at room temperature. For the inhibition curves, ion currents were evoked by switching from control solution to a solution containing 100 μM AMPA and 30 μM cyclothiazide (CTZ). After 5 min of AMPA/CTZ perfusion the solution was switched to AMPA/CTZ plus various concentrations of LY3130481 for 5 min. Inhibition was calculated from the current amplitude at the end of LY3130481 application and the current amplitude of the AMPA/CTZ response just before LY3130481application.. The potency of LY3130481 is calculated as follows. The steady-state current amplitude evoked by AMPA + CTZ in the presence of LY3130481 was normalized by that in the absence of LY3130481, and was plotted as the function of Log[LY3130481]. We used three-parameter sigmoidal curve fit method in Prism 6 software to calculate the IC50.

Selectivity assay by radioligand displacement This assay was conducted by Cerep (Celle-Lévescault, France). The membrane fraction from rat brain or cells with heterologously-expressed recombinant receptors was incubated with the radioligand shown in Table 2 in the presence or absence of 1 or 10 μM LY3130481 for 30-120 min at 4°C, RT or 37°C. The binding reaction was terminated with rapid filtration, and the radioactivity retained on the filters, which is defined as total binding, were measured with a scintillation counter. Non-specific binding was determined by including excess concentration of cold competitors shown in Table 2. Specific binding was total binding subtracted by non-specific binding. The percent inhibition of specific binding by LY3130481 was calculated as:

100 – (Specific binding in the presence of LY3130481 / Specific binding in the absence of LY3130481 x 100)

Measurement of LY3130481 concentration in hippocampal slices Transverse hippocampal slices (400 μm thick) were prepared from 3-6 weeks old Sprague Dawley rats and allowed to rest at room temperature in carbogenated recording solution: NaCl 124, $NaHCO_3$ 26, KCl 3, glucose 10, $CaCl_2$ 2.3, $MgCl_2$ 1.3 with 300-305 mOsm for 30 min as described above. The slices were transferred into a chamber with 1 μM LY3130481 in carbogenated recording solution. Ten slices (30-60 mg hippocampal tissue) were removed from LY3130481-containing solution washed with ~50 ml of carbogenated recording solution three times, and stored at -80°C. The slices were homogenized in 300 μl of water/methanol (4:1, v/v). Stock solutions containing 1 mg/ml of LY3130481 were diluted to produce working solutions which were then used to fortify control brain homogenate to produce calibration standards with concentrations ranging from 1 to 5000 ng/ml. Aliquots of each study sample, calibration standard, and control sample were then transferred to 96-well plates, mixed with acetonitrile/methanol (1:1, v/v) containing an internal standard to precipitate sample proteins, and centrifuged. The resulting supernatants were subjected to liquid chromatography with tandem mass spectrometry analysis using an Applied Biosystems/MDS Sciex API 4000 (Foster City, CA) equipped with a TurboIonSpray interface, and operated in positive ion mode. The analytes were chromatographically separated with a gradient liquid chromatography system and detected and quantified with selected reaction monitoring (M+H)+ transitions specific to LY3130481, m/z 383.1 > 232.1. The free fraction of LY3130481 was measured by mixing placing mixttures of LY3130481 and brain into a dialysis block with buffer on the other side. After 4.5-h incubation, the samples were taken from both sides. Fraction unbound is calculated by dividing the LC/MS/MS area of the buffer side by the LC/MS/MS area of the protein side.

General statistical considerations: in vitro data Experiments with the FLIPR system were conducted blind and with randomization. All other in vitro experiments were semi-randomized without blinding to condition. Group sizes were prospectively determined on the basis of previous publications assessing concentration response curves [29]. Decisions regarding statistical analyses were based upon the nature of the data, distributions, homogeneity of variance, and other statistically-validated criteria. All data for ANOVA were evaluated for normally-distributed functions and the statistical analysis was handled accordingly as noted. All data are provided with estimated variation which is taken into account in statistical treatments. Specific cases are described in the figure legends and table captions. Data exclusion on occasion was determined by a priori and statistically-accepted outlier analyses as described in Patch Clamp Electrophysiology section.

Animal studies Studies were performed according to the guidelines set forth by the National Institutes of Health and implemented by the Animal Care and Use Committee of Eli Lilly and Company and collaborative research institutes. All rodents used in this report were male. Group sizes were determined by a priori experience in the labs in which they were conducted as appropriately powered to identify standard of care anticonvulsant and motor-impairment. Animals were randomly-assigned to treatment groups by independently drawing animals from their housing cages. For animal studies, the experimental observers were blinded to the treatments. In all studies, homogeneity of variances were assessed to determine the proper statistical treatment. For quantal data, no variances were created; data were replicated to assure reliability of findings as noted in figure captions.

Pentylenetetrazole-Induced Seizures We administered LY3130481 (orally) or GYKI52466 (intraperitoneally) 30 min before subcutaneous PTZ dosing (35 mg/kg) to evaluate their ability to prevent or dampen seizures induced in male Sprague-Dawley rats (90-100 g, ~5 weeks old). The rats were used at this weight so as to better accommodate them on the inverted-screen test described below. After dosing, animals were observed for 30 minutes after PTZ for clonus (defined as clonic seizure of forelimbs and hindlimbs during which the mouse demonstrates loss of righting). The dose of PTZ was based upon estimated ED_{90} values for PTZ in these assays. The percentage of rats protected from seizure induction was assessed across doses from no effect to full protection and the data were analyzed by Fisher's Exact probability test as per typical for quantal data. Comparable studies were conducted in male, TARP γ-8 $^{-/-}$ and γ-8$^{+/+}$ mice [17]. Mice were treated as described for rats above except that they were given 70 mg/kg PTZ.

Pentelentetrozole (PTZ)-induced kindled seizures and motor impairment assessments. Male, CD1 mice were given PTZ (45 mg/kg, s.c.) every other day as described[30]. Mice were dosed on days 1,3, and 5 and then divided into groups of 8 or 9 and tested on day 8 with either PTZ alone (45 mg/kg, s.c.), perampanel (30 mg/kg, i.p., 30 min prior) + PTZ, or LY3130481 (10 mg/kg, i.p., 30 min prior) + PTZ. Mice were then observed for 30 min for the occurrence of convulsions. Behavioral observations were conducted by a blinded but trained observer using a 3-point rating scale where 0 = no difference to vehicle side-by-side; 1 =reduced movement and/or slight gait abnormality; and/or leaning as exemplified by 100 mg/kg lamotrigine, i.p., 30 min prior; 2 = more severe aspects of rating #1 that can include falling as exemplified by 500 mg/kg valproate, i.p. ., 30 min prior; and 3 = marked impairment, including periodic or complete loss of righting – exemplified by 1000 mg/kg valproate, i.p., 30 min prior. Seizure data were statistically evaluated by comparing seizure prevalence in vehicle-treated mice to

drug-treated mice with Fisher's Exact probability test. Behavioral data were evaluated by ANOVA with post-hoc Dunnett's test.

Mesial temporal lobe epilepsy model The MTLE mouse model recapitulates many of the characteristics observed in human patients with temporal lobe epilepsy (TLE). The MTLE mouse is characterized by an initial neurotoxic event, a unilateral intrahippocampal injection of kainic acid (KA) into the dorsal hippocampus, which induces non-convulsive SE lasting several hours. This initial event is followed by a latent phase. Two to three weeks after KA injection, spontaneous recurrent hippocampal paroxysmal discharges (HPD) are only recorded in the epileptic hippocampus and remain stable and stereotyped for the whole life of the animal [18,31]. These HPDs occur spontaneously about 30-60 times per hour when the animals are in a state of quiet wakefulness, generally last 15-20 sec and are associated with behavioral arrest and/or mild motor automatisms. Adult, male C57/Bl6 mice were stereotaxically injected with kainate (1 nmol in 100 nL) and implanted with 1 bipolar electrode in the dorsal hippocampus, and then allowed to recover for four weeks. A dose effective against 6 Hz-induced seizures of LY3130481 was then evaluated in 4 MTLE mice. Each mouse was used as their own control (vehicle). Digital EEG recordings were performed on freely moving animals for a 20 min pre-injection reference period and 90 min post dosing. Data were analyzed for the period of 10 min before and 10 min after peak time of effect of LY3130481 as observed in the 6 Hz model (15 min). Any accompanying effect on animal behavior was recorded. Data are presented as the raw number of HPDs during the analyzed 20 min period (10 min before and 10 min after) and expressed as a mean + S.E.M. and were statistically evaluated by Student's t-test.

Inverted Screen Test Sedative/ataxic effects were evaluated as described. Briefly, 30 minutes after LY3130481 application, but before dosing the animals with PTZ, an inverted screen test was carried out as described [4]. The apparatus is made of six 11 cm × 14 cm (mouse) or four 13 cm × 16 cm squares (rat) of round hole, perforated, stainless steel mesh (18 holes/square inch, 3/16-inch diameter, 1/4-inch staggered centers, 50% open area) that are mounted 15 cm apart on a metal rod, 35 cm above the tabletop. On the day before the test, mice were placed on the screen, and the rod was rotated 180° over 2 to 3 seconds. The amount of time it took for the test subject to climb to the top of the screen was recorded. For the test subjects that hung on the bottom for the maximum of 60 seconds, a 60-second score was recorded. A test with compound on board was studied the next day in the same manner. Animals were dosed orally with the LY3130481 or intraperitoneally with GYKI52466 and returned to their home cage. Twenty-five minutes after pretreatment, the animals were tested on the inverted

screen and were scored after 60 seconds as follows: 0 = climbed over, 50 = hanging on to screen, and 100 = fell off. After the inverted screen test, animals were dosed with PTZ in a volume of 1 ml/kg and placed in an observation cage (40.6 × 20.3 × 15.2 cm) with a floor containing 0.25 inches of wood-chip bedding material**.** Mean + SEM data were analyzed by ANOVA and individual contrasts were evaluated by post-hoc Dunnett's test.

Locomotor activity assessments. Male,CD1 mice, were injected (i.p.) with vehicle, LY3130481 or perampanel and then evaluated for locomotor activity changes for 45 min post dosing. Activity was accessed in a translucent polypropylene (40.6 x 20.3 x 15.2 cm, no bedding) cage. Distance traveled and vertically-directed behaviors were measured by the breaking of photobeams (San Diego Instruments). Data were analyzed by ANOVA followed by post-hoc Dunnett's tests. Adult, male Wistar rats (4-8 month old) were anesthetized and surgically prepared with an abdominally implanted miniature transmitter (PDT4000 Starr Life Sciences) that permitted chronic recording of body motion[32,33]. Locomotor activity of the rat in it's individual home cage was monitored by telemetry signals detected using a radio–telemetry receiver located beneath the cage (ER-4000, Minimitter, Bend, OR) and activity of the animal tracked continuously for 19 hours. The accumulated counts were collected using SCORE-2004 software and compared to vehicle controls. Statistical significance was calculated by analysis of covariance (ANOVA) using the corresponding pre-dose baseline period as the covariate. Drug mediated effects were measured following oral administration of LY3130418 or perampanel.

Amygdala kindling Male Wistar rats were prepared with bipolar electrodes aimed at one hemisphere of the basolateral amygdala (AP -2.2 , ML -4.8, DV -8.5 mm, relative to bregma) for electrical stimulation and EEG recording. After post-operative recovery, electrical kindling begins, where a subthreshold constant current (400μA, 1 ms, monophasic square-wave pulses, 60 Hz for 1 sec) is given once a day Monday-Friday for about 4-6 weeks until a rat is fully kindled. These rats began kindling at ~9 weeks of age at ~300g. At the time of testing with LY3130481, the animals were ~26 weeks old and 450-500g. A fully kindled rat has experienced 10 consecutive stage 5 seizures or 10 of its last 12 were stage 5 according to the Racine Scale [34]. Of the 12 fully kindled rats so created, eight rats were selected and randomized to initial compound treatment groups. On test day rats were dosed LY3130481 (i.p.) 30 minutes prior to stimulation with 400μA current. The percentage of the eight rats not exhibiting seizures was assessed post stimulation. Valproic acid (300 mg/kg, i.p.) was used as a positive control. These quantal data were analyzed with Fisher's Exact probability test for significance at $p<0.05$.

Immunoprecipitation GluA2 antibody (NeuroMab, clone L21/32) was covalently conjugated onto the magnetic beads with Protein A and Protein G as follows. Equal volume (80 µl each) of Dynabeads Protein A and Protein G (Life Technologies) were washed with PBS and then incubated with 20 µg of the GluA2 antibody for >8 h with gentle mixing at 22^{o}C. The beads were washed with citrate-phosphate buffer at pH 5.0, and then with 0.2 M triethanolamine pH 8.2. The antibodies on Protein A/G were cross-linked with 20 mM DMP (dimethyl pimelimidate x 2 HCl) in 0.2 M triethanlamine, pH 8.2 for 30 min at 22oC. The reaction was chased by the incubation with 50 mM Tris pH 7.5 for >15 min. The beads were washed by PBS containing 0.01% Tween-20. Post-nuclear P2 pellet from 1 g of rat hippocampi was prepared as described in [24]. The P2 pellet was resuspended in x20 original tissue volume of PBS, and aliquoted 2 ml each. Add an AMPA receptor antagonist at the concentration with maximum inhibition in the aliquot (LY3130481: 10 µM, GYKI: 40 µM, NBQX: 20 µM). Solubilize the membrane by the incubation with 1% CHAPS at 4^{o}C for 1 h, and then remove the unsolubilized materials by centrifugation at 100,000 x g at 4^{o}C for 1 h. The resultant lysate was incubated with the magnetic beads with the anti-GluA2 (1 µg antibody) for 2-3 h. The beads were washed three times with PBS + 1% CHAPS containing the corresponding AMPA receptor antagonist. The immunoprecipitated proteins were eluted with 20 µl of Laemmli buffer without reducing reagent at 55^{o}C for 30 min to minimize the antibody contamination from the beads. The eluted samples were reduced with DTT after transferred into new tubes, and then were subjected to immunoblotting with anti-GluA1 (Millipore, AB1504), anti-γ-8 (Frontier Institute, TARP-g8 Rb Af1000), or anti-TARP (Upstate, 07-577) antibodies.

References

1 Huganir, R. L. & Nicoll, R. A. AMPARs and synaptic plasticity: the last 25 years. *Neuron* **80**, 704-717, doi:10.1016/j.neuron.2013.10.025 (2013).

2 Hibi, S. *et al.* Discovery of 2-(2-oxo-1-phenyl-5-pyridin-2-yl-1,2-dihydropyridin-3-yl)benzonitrile (perampanel): a novel, noncompetitive alpha-amino-3-hydroxy-5-methyl-4-isoxazolepropanoic acid (AMPA) receptor antagonist. *Journal of medicinal chemistry* **55**, 10584-10600, doi:10.1021/jm301268u (2012).

3 French, J. A. *et al.* Adjunctive perampanel for refractory partial-onset seizures: randomized phase III study 304. *Neurology* **79**, 589-596, doi:10.1212/WNL.0b013e3182635735 (2012).

4 Zwart, R. *et al.* Perampanel, an antagonist of alpha-amino-3-hydroxy-5-methyl-4-isoxazolepropionic acid receptors, for the treatment of epilepsy: studies in human epileptic brain and nonepileptic brain and in rodent models. *The Journal of pharmacology and experimental therapeutics* **351**, 124-133, doi:10.1124/jpet.114.212779 (2014).

5 Jackson, A. C. & Nicoll, R. A. The expanding social network of ionotropic glutamate receptors: TARPs and other transmembrane auxiliary subunits. *Neuron* **70**, 178-199, doi:10.1016/j.neuron.2011.04.007 (2011).

6 Partin, K. M., Patneau, D. K., Winters, C. A., Mayer, M. L. & Buonanno, A. Selective modulation of desensitization at AMPA versus kainate receptors by cyclothiazide and concanavalin A. *Neuron* **11**, 1069-1082 (1993).

7 Turetsky, D., Garringer, E. & Patneau, D. K. Stargazin modulates native AMPA receptor functional properties by two distinct mechanisms. *J Neurosci* **25**, 7438-7448 (2005).

8 Tomita, S. *et al.* Stargazin modulates AMPA receptor gating and trafficking by distinct domains. *Nature* **435**, 1052-1058 (2005).

9 Gardinier, K. M. *et al.* The Discovery of The First alpha-Amino-3-Hydroxy-5-Methyl-4-Isoxazolepropionic Acid (AMPA) Receptor Antagonist Dependent Upon Transmembrane AMPA Receptor Regulatory Protein (TARP) Gamma-8. *Journal of medicinal chemistry*, doi:10.1021/acs.jmedchem.6b00125 (2016).

10 Cokic, B. & Stein, V. Stargazin modulates AMPA receptor antagonism. *Neuropharmacology* **54**, 1062-1070 (2008).

11 Kott, S., Werner, M., Korber, C. & Hollmann, M. Electrophysiological properties of AMPA receptors are differentially modulated depending on the associated member of the TARP family. *J Neurosci* **27**, 3780-3789 (2007).

12 Schwenk, J. *et al.* Functional proteomics identify cornichon proteins as auxiliary subunits of AMPA receptors. *Science (New York, N.Y* **323**, 1313-1319 (2009).

13 Shi, Y. *et al.* Functional comparison of the effects of TARPs and cornichons on AMPA receptor trafficking and gating. *Proceedings of the National Academy of Sciences of the United States of America* **107**, 16315-16319 (2010).

14 Geiger, J. R. *et al.* Relative abundance of subunit mRNAs determines gating and Ca2+ permeability of AMPA receptors in principal neurons and interneurons in rat CNS. *Neuron* **15**, 193-204 (1995).

15 Kato, A. S. *et al.* Hippocampal AMPA Receptor Gating Controlled by Both TARP and Cornichon Proteins. *Neuron* **68**, 1082-1096 (2010).

16 Gill, M. B. *et al.* Cornichon-2 modulates AMPA receptor-transmembrane AMPA receptor regulatory protein assembly to dictate gating and pharmacology. *J Neurosci* **31**, 6928-6938 (2011).
17 Gleason, S. D. *et al.* Inquiries into the Biological Significance of Transmembrane AMPA Receptor Regulatory Protein (TARP) gamma-8 Through Investigations of TARP gamma-8 Null Mice section sign. *CNS & neurological disorders drug targets* **14**, 612-626 (2015).
18 Twele, F., Bankstahl, M., Klein, S., Romermann, K. & Loscher, W. The AMPA receptor antagonist NBQX exerts anti-seizure but not antiepileptogenic effects in the intrahippocampal kainate mouse model of mesial temporal lobe epilepsy. *Neuropharmacology* **95**, 234-242, doi:10.1016/j.neuropharm.2015.03.014 (2015).
19 Tomita, S. & Castillo, P. E. Neto1 and Neto2: auxiliary subunits that determine key properties of native kainate receptors. *The Journal of physiology* **590**, 2217-2223, doi:10.1113/jphysiol.2011.221101 (2012).
20 Maher, M. P. *et al.* Discovery and Characterization of AMPA Receptor Modulators Selective for TARP-gamma8. *The Journal of pharmacology and experimental therapeutics* **357**, 394-414, doi:10.1124/jpet.115.231712 (2016).
21 Witkin, J. M. & Gardinier, K. M. A Comment on "Discovery and Characterization of AMPA Receptor Modulators Selective for TARP-gamma8". *The Journal of pharmacology and experimental therapeutics* **358**, 502-503, doi:10.1124/jpet.116.234419 (2016).
22 Sommer, B. *et al.* Flip and flop: a cell-specific functional switch in glutamate-operated channels of the CNS. *Science (New York, N.Y* **249**, 1580-1585 (1990).
23 Burgess, D. L., Gefrides, L. A., Foreman, P. J. & Noebels, J. L. A cluster of three novel Ca2+ channel gamma subunit genes on chromosome 19q13.4: evolution and expression profile of the gamma subunit gene family. *Genomics* **71**, 339-350 (2001).
24 Kato, A. S., Siuda, E. R., Nisenbaum, E. S. & Bredt, D. S. AMPA receptor subunit-specific regulation by a distinct family of type II TARPs. *Neuron* **59**, 986-996 (2008).
25 Rouach, N. *et al.* TARP gamma-8 controls hippocampal AMPA receptor number, distribution and synaptic plasticity. *Nature neuroscience* **8**, 1525-1533 (2005).
26 Miledi, R., Eusebi, F., Martinez-Torres, A., Palma, E. & Trettel, F. Expression of functional neurotransmitter receptors in Xenopus oocytes after injection of human brain membranes. *Proceedings of the National Academy of Sciences of the United States of America* **99**, 13238-13242, doi:10.1073/pnas.192445299 (2002).
27 Miledi, R., Palma, E. & Eusebi, F. Microtransplantation of neurotransmitter receptors from cells to Xenopus oocyte membranes: new procedure for ion channel studies. *Methods Mol Biol* **322**, 347-355, doi:10.1007/978-1-59745-000-3_24 (2006).
28 Eusebi, F., Palma, E., Amici, M. & Miledi, R. Microtransplantation of ligand-gated receptor-channels from fresh or frozen nervous tissue into Xenopus oocytes: a potent tool for expanding functional information. *Progress in neurobiology* **88**, 32-40, doi:10.1016/j.pneurobio.2009.01.008 (2009).
29 Kato, A. S. *et al.* New transmembrane AMPA receptor regulatory protein isoform, gamma-7, differentially regulates AMPA receptors. *J Neurosci* **27**, 4969-4977 (2007).
30 Kaminski, R. M., Witkin, J. M. & Shippenberg, T. S. Pharmacological and genetic manipulation of kappa opioid receptors: effects on cocaine- and pentylenetetrazol-induced convulsions and seizure kindling. *Neuropharmacology* **52**, 895-903, doi:10.1016/j.neuropharm.2006.10.007 (2007).
31 Suzuki, F., Junier, M. P., Guilhem, D., Sorensen, J. C. & Onteniente, B. Morphogenetic effect of kainate on adult hippocampal neurons associated with a prolonged expression of brain-derived neurotrophic factor. *Neuroscience* **64**, 665-674 (1995).

32 Harkin, A., O'Donnell, J. M. & Kelly, J. P. A study of VitalView for behavioural and physiological monitoring in laboratory rats. *Physiology & behavior* **77**, 65-77 (2002).
33 Phillips, K. G. *et al.* Differential effects of NMDA antagonists on high frequency and gamma EEG oscillations in a neurodevelopmental model of schizophrenia. *Neuropharmacology* **62**, 1359-1370, doi:10.1016/j.neuropharm.2011.04.006 (2012).
34 Racine, R. J. Modification of seizure activity by electrical stimulation. II. Motor seizure. *Electroencephalography and clinical neurophysiology* **32**, 281-294 (1972).

Supplementary Legends

Supplementary Figure 1 LY3130481 potently blocked glutamate-evoked steady-state currents in cells with GluA1i + γ-8, but not with GluA1i + the other TARP or CNIH-2. (a) Traces of glutamate- or kainate-evoked currents in HEK293T cells co-transfected with GluA1i alone or GluA1i and an auxiliary subunit as indicated. See Fig 2a for concentration-response curves (CRC). Glutamate application evoked rapid inward current, which desensitized and reached steady-state as long as glutamate was applied. The glutamate application induced resensitization, i.e. gradual increase of desensitized glutamate-evoked currents, in γ-4, γ-7 and γ-8 co-transfectants as published [1]. We also show the summaries of the amplitude of glutamate-evoked steady state currents **(b)**, I_{KA} / $I_{Glu\ steady\text{-}state}$ ratio **(c)** and resensitization indices (See Methods) **(d)** recorded from the cells used for the CRCs in Figure 2A. We verified co-transfection of auxiliary subunits as follows. γ-2: large (>200 pA) glutamate-evoked steady-state currents (b) and high kainate efficacy ($I_{KA}/I_{Glu\ steady\text{-}state}$) (c) [2-4], γ-3: high kainate efficacy (c) [5], γ-4, γ-7, γ-8: Resensitization [1] (d), CNIH-2: Large (>200 pA)glutamate-evoked currents (b) [6]. The averaged amplitude of steady-state glutamate-evoked currents for GluA1 alone was ~40 pA (b) [7] and did not reach 150 pA. This figure is associated with Fig. 2a.

Supplementary Figure 2 Perampanel antagonized AMPA receptors with TARPs. (a, d) Traces of glutamate-evoked currents in HEK293T cells co-transfected with GluA1i alone or GluA1i and an auxiliary subunit as indicated in the presence of GYKI53784 **(a)** or perampanel **(d)**. **(b, e)** Concentration-response curves for inhibition of glutamate-evoked currents by GYKI **(b)** or perampanel **(e)**. The potencies of GYKI53784 and perampanel to γ-2- or γ-8-containing GluA1i were somewhat higher than GluA1i alone (See also Supplemental Table 1b and 1c) [8]. **(c, f)** Co-transfection of γ-2 or γ-8 in panel a, b, d and e was verified by larger (>200 nA) glutamate-evoked steady-state currents than GluA1 alone (30~40 pA).

Supplementary Figure 3 LY3130481 blocked γ-8-containing AMPA receptors without GluA subunit selectivity Glutamate-evoked currents in HEK293T cells co-transfected with GluA2i, GluA3i, GluA4i or GluA1o with or without a TARP. LY3130481 blocked all AMPA receptor subunits if γ-8 was co-expressed. **(a)** Raw traces of glutamate-evoked currents in with various concentrations of LY3130481. The summaries of the amplitude of glutamate-evoked steady state currents from GluA2i- **(b)**, GluA3i- **(c),** GluA4i- **(d)** and GluA1o- **(e)** expressing cells recorded for the CRCs in main Fig 2b-e. The large glutamate-evoked currents confirmed functional expression of TARPs with AMPA receptor principal subunits **(b-e)**. This figure is associated with Fig. 2b-e.

Supplementary Figure 4 LY3130481 blocked γ-8 containing GluA1/2 heteromers, and the stoichiometry of γ-8 to AMPA receptors regulated the pharmacology of LY3130481. **(a)** Traces of glutamate-evoked currents in HEK293T cells co-expressing indicated AMPA receptors and their auxiliary subunits, LY3130481 potently and selectively blocked GluA1i/2i heteromers if γ-8 was expressed. The summaries of I_{KA} / $I_{Glu\ steady\text{-}state}$ ratio **(b)**, I-V relationship of glutamate-evoked responses before LY3130481 application **(c)** with rectification index, $I_{Glu\ (-80\ mV)}$ / $I_{Glu\ (+40\ mV)}$ **(d)**, resensitization index **(e)** and the amplitude of glutamate-evoked steady state currents **(f)** measured from the recordings used for the CRCs in Fig 2e and 2f. TARP incorporation was verified by the high I_{KA} / $I_{Glu\ steady\text{-}state}$ ratio (b) [3-5,9,10]. Efficient GluA2i incorporation in the heteromers was verified by linear I-V relationships (c, d) [11,12]. CNIH-2 incorporation with γ-8 was verified by no resensitization and high I_{KA} / $I_{Glu\ steady\text{-}state}$ ratio (b, d) [1]. Formation of the AMPA receptors with low γ-8 stoichiometry by co-expression of GluA1i/ γ-8 tandem construct with GluA was verified by no resenstization and larger $I_{Glu\ steady\text{-}state}$ (b, f) [9,10]. Linear I-V relationship and high I_{KA} / $I_{Glu\ steady\text{-}state}$ ratio were also used for the verification in the subset of the recorded cells [10]. This figure is associated with Fig. 2e, 2f. **(g)** Co-expression of CNIH-2 with GluA2i and γ-8 further reduced efficacy of LY3130481 compared to GluA2i + γ-8, which is similar to GluA1i shown in Fig. 2f. **(h, i)** The summary of I_{Glu} / I_{KA} ratio and resensitization profiles of the individual transfectants used for the CRC shown in (g). Co-expression of all of GluA2i, γ-8 and CNIH-2 in GluA2i + γ-8 + CNIH-2 transfectatns was confirmed by larger I_{KA} / I_{Glu} ratio than GluA2i + CNIH-2 (h) and lack of resensitization (i). LY3130481 showed lower efficacy in GluA2 + γ-8 (Fig. 2b) compared to the other AMPA receptor subunits associated with γ-8 (Fig. 2a, 2c-2e). Reducing γ-8 stoichiometry on AMPA receptors by either co-expression of CNIH-2 or using GluA1/γ-8 tandem construct also lowered the efficacy of LY3130481 (Fig. 2f, 2g). The low LY3130481 efficacy on GluA2 + γ-8 could be explained by lower γ-8 stoichiometry on GluA2 than on GluA1. However this possibility is not likely. GluA2 + γ-8 displayed resensitization (Supplementary Fig. 3a, 4i), which is the signature response of the AMPA receptor with high-stoichiometric γ-8 [10]. Co-expression of CNIH-2 with GluA2 + γ-8 eliminated resensitization but retained high I_{KA}/I_{Glu} ratio (h, i), which is the signature of AMPA receptors with low stoichiometric γ-8 [10], and this further reducted LY3130481 efficacy (g, Supplementary Table 1a). These observations strongly suggest that GluA2 + γ-8 forms GluA2 with high-stoichiometric γ-8, and the lower LY3130481 efficacy in GluA2 + γ-8 is due to intrinsic properties of the channel complex.

Supplementary Figure 5 TM3 and TM4 in γ-8 additively contribute to the potent antagonist properties of LY3130481 (a) Traces of glutamate-evoked currents recorded from heterologously

expressed GluA1i + designated TARP or γ-8 / γ-4 chimeras perfused with LY3130481. **(b)** The amplitudes of steady-state currents evoked by glutamate are shown (logarithmic scale). All chimeras showed much larger current amplitude than GluA1i expressed alone. **(c)** Resensitization indices for chimera are shown. All chimeras with GluA1i yielded similar resensitization profiles as the parental γ-8 and γ-4, but much larger than GluA1i alone. These observations confirm that chimeras confer TARP properties comparable to γ-8 and γ-4 (b, c). **(d)** Concentration response curves (CRC) of LY3130481 for the chimeras coexpressed with GluA1i. Relative amplitudes of glutamate-evoked steady-state currents are plotted as a function of LY3130481 concentration. **(e)** The potency of LY3130481 for each chimera is shown by IC_{50} values with schematic representation of the chimeras. Swapping either TM3 or TM4 from γ-8 with those from γ-4 resulted in partial reduction in potency. When TM3 and TM4 form γ-4 were replaced with those from γ-8 similar potency values to γ-4 were seen. Error bars indicate SEM. Parentheses indicate the number of the recorded transfectants. *; $p<0.001$ compared to GluA1 + γ-8, #; $p<0.001$ compared to GluA1 + γ-4 with Dunnett's test. This figure is the preliminary basis of Fig. 2i.

Supplementary Figure 6 LY3130481 potently blocks γ-4 with γ-8 TM3 + TM4(a) Traces of glutamate-evoked currents through GluA1i co-expressed with γ-4 / γ-8 chimeras under perfusion with LY3130481 at designated concentrations. **(b)** The amplitudes of steady-state currents evoked by glutamate are shown. All chimeras gave much larger current amplitude than GluA1i alone. **(c)** The extents of resensitization for all chimeras were similar to γ-4 and γ-8, but were much larger than GluA1i alone. All chimeras modulated AMPA receptor functions as well as γ-8 and γ-4 (b, c). **(d)** Relative amplitudes of glutamate-evoked steady-state currents are plotted as a function of LY3130481 concentration. **(e)** The potency of LY3130481 was shown by IC_{50}. Swapping either γ-4 TM3 or TM4 with γ-8 partially restored the potency. Mutants of γ-4 containing TM3 and TM4 from γ-8 showed similar potencies to γ-8. Error bars indicate SEM. Parentheses indicate the number of the recorded transfectants. *; $p<0.001$ compared to GluA1 + γ-8, #; $p<0.001$ compared to GluA1 + γ-4 with Dunnett's test. **(f)** Alignment of the amino acid sequences at TM3 and TM4 of Type I TARPs [13] with colors at non-conserved amino acid residues between γ-8 and the other Type I TARPs. This figure is the preliminary basis of Fig $2h_2$.

Supplementary Figure 7 The two amino acids uniquely located in TM3 and TM4 of γ-8 regulated the potency of LY3130481 (a, b) Traces of glutamate-evoked currents through GluA1 co-expressed with γ-8 **(a)** or γ-4 **(b)** point mutants under perfusion with LY3130481 at the designated concentrations. The amplitudes of steady-state currents and the extent of resensitization evoked by glutamate are shown

below the traces. All mutants gave much larger current amplitude and resensitization than GluA1i alone. These observations confirm that the point mutants have TARP functions. **(c, d)** Relative amplitudes of glutamate-evoked steady-state currents through GluA1i with γ-8 mutants **(c)** or with γ-4 mutants **(d)** are plotted as a function of LY3130481 concentration. (e, f) The amino-acid sequences of the γ-8 (e) and γ-4 (f) point mutants tested for the potency and efficacy of LY3130481 in Fig. 2i and 2j.

Supplementary Figure 8 LY3130481 blocks glutamate-evoked currents through GluA1i co-expressed with γ-2 with substitutions of critical amino acids **(a)** The amino-acid sequences of the γ-2 point mutants tested for the potency and efficacy of LY3130481 in Fig. 2k **(b)** Traces of glutamate-evoked currents through GluA1 + γ-2 point mutants under the perfusion with LY3130481. **(c)** The amplitudes of steady-state currents and the ratios of I_{KA} to I_{Glu} are shown . All of these γ-2 point mutants have TARP functions, since they gave much larger current amplitude and I_{KA}/I_{Glu} than GluA1i alone [2-4]. **(d)** Relative amplitudes of glutamate-evoked steady-state currents through GluA1 with γ-2 mutants are plotted as a function of LY3130481 concentration. The summary of the potency values is shown in main Fig. 2j. Error bars indicate SEM. Parentheses indicate the number of the recorded transfectants. **(e)** Schematic representation of TARP topology with the location of the critical residues for selectivity of LY3130481. This figure is associated with Fig. 2i, 2j, 2k.

Supplementary Figure 9 Brain region specific and γ-8-dependent action of LY3130481 in acutely isolated rodent neurons (a) Typical traces recorded from acutely isolated rat neurons associated with Fig 3a. All glutamate-evoked responses under this experimental condition were blocked by GYKI 53784 (40 μM), indicating they were AMPA receptor-mediated. LY3130481 blocked responses in hippocampal and cortical neurons but not in Purkinje neurons. This panel is associated with Fig 3a. **(b)** Representative traces recorded from acutely isolated hippocampal neurons from γ-$8^{+/+}$ or γ-$8^{-/-}$ mice. The concentration-dependent blockade of AMPA receptor-mediated responses by LY3130481 was abolished in γ-8 deficient mice. This panel is associated with Fig 3b. **(c)** Glutamate-evoked responses recorded from acutely isolated rat neurons from hippocampus, cortex and cerebellar Purkinje cells in the presence of various concentrations of perampanel. Complete current blockage by high concentration of GYKI and perampanel confirmed the glutamate-evoked responses in this condition were fully AMPA receptor-mediated [14]. **(d)** CRCs for the inhibition of glutamate (1 mM)-evoked steady-state currents by perampanel on acutely-isolated rat neurons No brain-region selectivity was observed.

Supplementary Figure 10 Gradual blockage of hippocampal field EPSP by LY3130481 seems due to its slow penetration into the slices. **(a)** LY3130481 quickly blocked AMPA receptor mediated responses in the hippocampal neurons isolated from hippocampus. Traces showing the time course of the blockage of glutamate-evoked responses by LY3130481. Note that the glutamate-evoked responses were fully AMPA receptor-mediated, as GYKI53784 completely blocked the response. **(b)** Summary of the relative amplitude of the glutamate-evoked steady-state currents recorded from 3 isolated hippocampal neurons plotted as a function of time after the perfusion of 0.1 μM LY3130481 shown in a. The time constant was calculated by fitting with one-phase decay curve. Note that the antagonistic action of LY3130481 is fairly quick (τ = 0.2 min) for isolated neurons, which are free from physical barriers such as glia and/or connective tissues. **(c)** The time course of the LY3130481 penetration into the hippocampal slices The slices were prepared with the same procedure as that for fEPSP recordings shown in Fig. 3C and 3D, and soaked in the carbogenated buffer with 1 μM LY3130481. The slices were sampled at various time points, and weighed. The total concentration of LY3130481 in each samples were measured (Left Y axis). Since the free fraction of LY3130481 in brain tissues were ~1%, we calculated the approximate concentration of free LY3130481 in hippocampal slices and showed at right Y axis. The time constant was calculated by fitting with single-phase decay curve. It took quite long for LY3130481 to penetrate into brain slices (τ = 52 min) (n = 2). The kinetics of LY3130481 penetration fits well with that of fEPSP blockage shown in Fig3c_2 and Fig 3d_1. In addition, the approximate concentration of free LY3130481 in hippocampal slices roughly fitted with the extent of $I_{Glusteady\text{-}state}$ and fEPSP inhibition (Fig. 3a, 3b, 3d_2). We concluded that the slow action of LY3130481 on the fEPSP recorded in hippocampal slices were due to the slow onset of compound penetration.

Supplementary Figure 11 Systemically administered LY3130481 did not block AMPA- or NMDA-evoked firing in the red nucleus. (a) A multi-barrel glass recording micropipette as inserted into the red nucleus area of anesthetized rats, and extracellular potentials were recorded with alternating iontophoretic applications of AMPA and NMDA. Firing rate and field potential were plotted as a function of time. We chose the red nucleus for the in vivo recording as this region expresses both γ-8 lacking AMPA receptors and functional NMDA receptors [15]. Cerebellar neurons were not readily amenable for recording under these conditions, since NMDA receptors in Purkinje neurons are at minimum level [16]. Red nucleus neurons show high frequency spontaneously firing as shown consistent with previous reports [17,18]. The firing rate was increased by iontophoretic applications of AMPA and NMDA. **(b)** The ratio of the AMPA- to NMDA-evoked firing rate was not changed by 1 or 3 mg/kg LY3130481, doses

which efficaciously suppressed AMPA-evoked hippocampal firing. GYKI53784 significantly decreased the AMPA to NMDA ratio of evoked firing (main Fig. 3e). **(c)** The γ-8 mRNA level in the red nucleus is below detectable levels (Allen Brain Atlas database).

Supplementary Figure 12 The mechanism of TDAA action is not likely the result of LY3130481-stimulated dissociation of γ-8 from AMPA receptors (a) (Top panels) Sequentially-recorded traces of glutamate and kainate-evoked currents from GluA1 + γ-8 expressing cells before, during and after the application of LY3130481. (Bottom panels) Traces of glutamate-evoked currents from GluA1, GluA2 + γ-8 and GluA2 with or without LY3130481 **(b)** Resensitization indices of glutamate-evoked currents before and after the application of LY3130481 LY3130481 reduced the resensitiztion for both GluA1 and GluA2 with γ-8. Error bars indicate SEM. Parentheses indicate the number of the recorded transfectants. Asterisk indicates $p<0.01$ with paired t-test. **(c, d)** Steady-state current amplitudes evoked by glutamate before and after the application of LY3130481 for GluA1 ± γ-8 **(c)** or GluA2 ± γ-8 **(d)** are compared with those for GluA1 or GluA2 alone. Note that the residual currents after the maximum inhibition by LY3130481 were significantly larger than GluA1 or GluA2 alone. Error bars indicate SEM. Parentheses indicate the number of the recorded transfectants. The inhibition by LY3130481 is statistically analyzed with paired-t-test. The comparison of γ-8 containing AMPA receptor with LY3130481 and AMPA receptor alone is performed with unpaired t-test. Asterisk indicates $p<0.05$. Error bars indicate SEM. Parentheses indicate the number of the recorded transfectants. Asterisk indicates $p<0.001$ with Turkey's test. **(e)** I_{KA} / I_{Glu} ratios of GluA1 + γ-8 during and after LY3130481 are compared with GluA1 alone. The characteristics of the residual currents from γ-8-containing GluA1 or GluA2 after LY3130481 applications were very different from GluA1 or GluA2 alone (c-e). Error bars indicate SEM. Parentheses indicate the number of the recorded transfectants. **(f)** GluA1-containing protein complexes were immunoprecipitated from rat forebrain membrane fractions, and immunoblotted with GluA1 and TARPs. The ratio of co-immunoprecipitated γ-8 or γ-2/3/4 to GluA1 was not changed by LY3130481 or other AMPA receptor antagonist, GYKI or NBQX. There was no evidence that LY3130481 dissociates γ-8 from AMPA receptors.

Supplementary References

1 Kato, A. S. *et al.* Hippocampal AMPA Receptor Gating Controlled by Both TARP and Cornichon Proteins. *Neuron* **68**, 1082-1096 (2010).

2 Chen, L. *et al.* Stargazin regulates synaptic targeting of AMPA receptors by two distinct mechanisms. *Nature* **408**, 936-943 (2000).

3 Turetsky, D., Garringer, E. & Patneau, D. K. Stargazin modulates native AMPA receptor functional properties by two distinct mechanisms. *J Neurosci* **25**, 7438-7448 (2005).

4 Tomita, S. *et al.* Stargazin modulates AMPA receptor gating and trafficking by distinct domains. *Nature* **435**, 1052-1058 (2005).

5 Kott, S., Werner, M., Korber, C. & Hollmann, M. Electrophysiological properties of AMPA receptors are differentially modulated depending on the associated member of the TARP family. *J Neurosci* **27**, 3780-3789 (2007).

6 Schwenk, J. *et al.* Functional proteomics identify cornichon proteins as auxiliary subunits of AMPA receptors. *Science (New York, N.Y* **323**, 1313-1319 (2009).

7 Kato, A. S. *et al.* New transmembrane AMPA receptor regulatory protein isoform, gamma-7, differentially regulates AMPA receptors. *J Neurosci* **27**, 4969-4977 (2007).

8 Cokic, B. & Stein, V. Stargazin modulates AMPA receptor antagonism. *Neuropharmacology* **54**, 1062-1070 (2008).

9 Shi, Y. *et al.* Functional comparison of the effects of TARPs and cornichons on AMPA receptor trafficking and gating. *Proceedings of the National Academy of Sciences of the United States of America* **107**, 16315-16319 (2010).

10 Gill, M. B. *et al.* Cornichon-2 modulates AMPA receptor-transmembrane AMPA receptor regulatory protein assembly to dictate gating and pharmacology. *J Neurosci* **31**, 6928-6938 (2011).

11 Hollmann, M., Hartley, M. & Heinemann, S. Ca2+ permeability of KA-AMPA--gated glutamate receptor channels depends on subunit composition. *Science (New York, N.Y* **252**, 851-853 (1991).

12 Sommer, B., Kohler, M., Sprengel, R. & Seeburg, P. H. RNA editing in brain controls a determinant of ion flow in glutamate-gated channels. *Cell* **67**, 11-19 (1991).

13 Kato, A. S., Gill, M. B., Yu, H., Nisenbaum, E. S. & Bredt, D. S. TARPs differentially decorate AMPA receptors to specify neuropharmacology. *Trends in neurosciences* **33**, 241-248 (2010).

14 Ceolin, L. *et al.* A novel anti-epileptic agent, perampanel, selectively inhibits AMPA receptor-mediated synaptic transmission in the hippocampus. *Neurochemistry international* **61**, 517-522, doi:10.1016/j.neuint.2012.02.035 (2012).

15 Harris, N. C. & Davies, J. Cortically evoked excitatory synaptic transmission in the cat red nucleus is antagonised by D-AP5 but not by D-AP7. *Brain Res* **594**, 176-180 (1992).

16 Llano, I., Marty, A., Armstrong, C. M. & Konnerth, A. Synaptic- and agonist-induced excitatory currents of Purkinje cells in rat cerebellar slices. *Journal of Physiology* **434**, 183-213 (1991).

17 Yang, J. C., Fan, X. L., Song, X. A. & Li, Q. The role of different glutamate receptors in the mediation of glutamate-evoked excitation of red nucleus neurons after simulated microgravity in rat. *Neuroscience letters* **448**, 255-259, doi:10.1016/j.neulet.2008.10.044 (2008).

18 Kinney, G. G. Peripheral nicotine administration increases rubral firing rates in the urethane-anesthetized rat. *Neuroscience letters* **198**, 1-4 (1995).

Supplementary Tables

Supplementary Table 1a – Summary of the LY3130481 pharmacology for recombinant AMPA receptors with auxiliary subunits

	Log[IC50 (M)]		IC50	Imax (%)		nH			
	Mean	SEM	(nM)	Mean	SEM	Mean	SEM	R^2	n
GluA1i + γ-2	[A, B] -4.47	0.22	33000	85.5	24.8			0.902	6
GluA1i + γ-3	[A, B] -4.78	0.21	16000	55.8	11.3			0.861	6
GluA1i + γ-4	[A] -5.41	0.12	3900	90.5	5.7			0.927	6
GluA1i + γ-8	[B] -8.07	0.05	8.4	93.0	1.9	-1.126	0.128	0.962	12
GluA2i + γ-2	[C] -4.82	0.08	15000	81.4	6.6			0.975	5
GluA2i + γ-4	[C] -5.28	0.14	5200	51.6	4.1			0.957	3
GluA2i + γ-8	-7.77	0.07	16	75.3	1.8	-0.828	0.097	0.951	12
GluA3i + γ-4	[D] -5.10	0.30	8000	71.4	16.2			0.840	3
GluA3i + γ-8	-7.66	0.17	21	94.2	4.3			0.870	4
GluA4i + γ-2	[E] -5.11	0.65	7700	43.8	16.5			0.532	3
GluA4i + γ-4	[E] -5.87	0.20	1300	75.7	6.6			0.889	3
GluA4i + γ-8	-7.72	0.08	19	98.1	2.0			0.970	4
GluA1o + γ-2	[F] -4.41	0.41	39000	88.6	55.0			0.874	3
GluA1o + γ-4	[F] -5.39	0.19	4000	90.5	9.5			0.906	4
GluA1o + γ-8	-8.22	0.07	6.0	99.1	2.4			0.970	5
GluA1i + GluA2i + γ-8	[G] -8.05	0.05	8.8	[G] 89.7	2.0	-1.073	0.129	0.960	11
GluA1i + GluA2i + γ-8 + CNIH-2	-7.63	0.05	23	66.5	1.8	-1.721	0.297	0.936	12
GluA1i + GluA2i + γ-4 + CNIH-2	[G] -5.48	0.23	3200	59.3	6.5			0.887	3
GluA1i + GluA2i + γ-2 + CNIH-2	[G] -5.30	0.12	4900	40.9	2.7			0.971	3
GluA1i + γ-8 + CNIH-2	[H] -7.77	0.09	17	[A] 69.1	2.2	-0.868	0.141	0.919	11
GluA2i + γ-8 + CNIH-2	-7.53	0.11	29	[C] 54.4	1.6			0.926	6
GluA1i/γ-8 tandem	-8.42	0.05	3.7	96.5	1.4	-1.046	0.100	0.968	12
GluA1i/γ-8 tandem + GluA1i	[I] -7.89	0.04	12	[I] 82.2	1.2	-1.256	0.119	0.975	12
GluA1i/γ-8 tandem + GluA2i	[I] -7.90	0.07	12	[I] 75.3	2.3	-1.547	0.371	0.895	11

Values are listed when the R^2 of fitted curves were larger than 0.6. Hill coefficients (nH) were calculated by 4-parameter sigmoidal curve fit, only when we measured more than 12 concentration points. The rest of CRCs were fitted with 3-parameter sigmoidal curve fit, in which nH is fixed to -1. Group-to-group statistical significance was evaluated by ANOVA and then Tukey's test (multiple groups) or unpaired two-tailed t-test (two groups). Statistical comparison of Imax is performed among γ-8 containing AMPA receptors only, because the CRCs for the AMPA receptors with the other TARPs did not reach plateau even at the highest LY3130481 concentration. [A] $p<0.001$ compared to GluA1i + γ-8, [B] $p<0.05$ compared to GluA1i + γ-4, [C] $p<0.001$ compared to GluA2i + γ-8, [D] $p<0.001$ compared to GluA3i + γ-8, [E] $p<0.05$ compared to GluA4i + γ-8, [F] $p<0.001$ compared to GluA1o + γ-8, [G] $p<0.001$ compared to GluA1 + GluA2 + γ-8 + CNIH-2, [H] $p<0.05$ compared to GluA1 + γ-8, [I] $p<0.001$ compared to GluA1/γ-8 tandem. The number of cells recorded for which R^2 values were less than 0.6, GluA1i + γ-5: n = 3, GluA1i + γ-7: n = 8, GluA1i + GluA2i + CNIH-2: n = 3

Supplementary Table 1b –
Summary of the GYKI pharmacology for GluA1i with or without TARPs

	Log[IC50 (M)]		IC50	Imax (%)			
	Mean	SEM	(nM)	Mean	SEM	R^2	n
GluA1i + γ-2	[A] -6.01	0.04	970	100.3	1.6	0.996	3
GluA1i + γ-8	[A] -6.00	0.10	990	100.6	3.9	0.975	3
GluA1i	-4.93	0.14	11000	109.2	9.4	0.960	3

The CRCs were fitted with 3-parameter sigmoidal curve fit, and calculated IC_{50} and I_{max}. Post-hoc statistical significance test after ANOVA was carried out for Log[IC_{50}] by Tukey's test. [A] $p<0.001$ compared to GluA1i

Supplementary Table 1c –
Summary of the perampanel pharmacology for GluA1i with or without TARPs

	Log[IC50 (M)]		IC50	Imax (%)			
	Mean	SEM	(nM)	Mean	SEM	R^2	n
GluA1i + γ-2	[A] -6.76	0.05	170	99.0	2.2	0.991	4
GluA1i + γ-8	[A] -6.69	0.10	200	98.9	3.7	0.971	3
GluA1i	-5.97	0.18	1000	107.6	10.7	0.900	3

The CRCs were fitted with 3-parameter sigmoidal curve fit, and calculated IC_{50} and I_{max}. Post-hoc statistical significance test after ANOVA was carried out for Log[IC_{50}] by Tukey's test. [A] $p<0.05$ compared to GluA1i

Supplementary Table 1d –
Summary of the glutamate CRCs in the presence of LY3130481 for GluA1i + γ-8

[LY3130481]	Log[EC50 (M)]		Glu EC50	Emax (%)			
	Mean	SEM	(uM)	Mean	SEM	R^2	n
0 µM	-4.93	0.06	11	108.8	2.4	0.991	3
0.003 µM	-5.27	0.17	5.4	61.1	3.6	0.923	3
0.01 µM	-5.56	0.10	2.7	41.8	1.3	0.975	3
0.03 µM	-5.35	0.25	4.5	20.2	1.7	0.855	3
0.1 µM	-5.04	0.13	9.2	10.9	0.5	0.947	3

The CRCs were fitted with 3-parameter sigmoidal curve fit.

Supplementary Table 1e –
Summary of the LY3130481 pharmacology for GluA1i + TARP mutants

	Log[IC50 (M)]		IC50	Imax (%)			
	Mean	SEM	(nM)	Mean	SEM	R^2	n
GluA1i + γ-8 / γ-4(TM1)	[B] -7.73	0.10	18	94.8	2.7	0.962	3
GluA1i + γ-8 / γ-4(Ex1)	[B] -7.83	0.08	14	92.0	2.2	0.974	3
GluA1i + γ-8 / γ-4(TM34)	[A] -5.71	0.27	1900	61.2	7.0	0.801	3
GluA1i + γ-8 / γ-4(C-term)	[B] -7.54	0.12	28	89.5	3.2	0.968	3
GluA1i + γ-8 / γ-4(TM3)	[A, B] -6.31	0.11	490	94.8	3.9	0.945	4
GluA1i + γ-8 / γ-4(Ex2)	[B] -7.74	0.10	18	94.3	2.5	0.954	3
GluA1i + v-8 / γ-4(TM4)	[A, B] -6.86	0.09	130	98.4	2.9	0.967	3
GluA1i + γ-8 / γ-4(TM3+4)	[A] -5.58	0.18	2600	62.1	5.3	0.923	3
GluA1i + γ-4 / γ-8(TM1)	[A] -5.22	0.15	6100	78.5	8.0	0.948	3
GluA1i + γ-4 / γ-8(Ex1)	[A] -5.60	0.23	2500	83.4	9.1	0.860	3
GluA1i + γ-4 / γ-8(TM34)	[B] -7.63	0.07	23	95.6	1.9	0.982	3
GluA1i + γ-4 / γ-8(C-term)	[A] -5.55	0.16	2700	80.5	6.0	0.927	3
GluA1i + v-4 / γ-8(TM3)	[A, B] -6.60	0.08	250	99.0	2.8	0.969	4
GluA1i + γ-4 / γ-8(Ex2)	[A] -5.74	0.13	1800	85.7	4.5	0.945	3
GluA1i + γ-4 / γ-8(TM4)	[A, B] -6.58	0.14	260	95.0	4.0	0.939	3
GluA1i + γ-4 / γ-8(TM3+4)	[B] -7.54	0.15	29	85.7	3.6	0.919	3
GluA1i + γ-8(I159V)	[B] -7.61	0.07	24	93.4	1.8	0.981	3
GluA1i + γ-8(G161S)	[B] -7.63	0.07	23	90.9	1.7	0.984	3
GluA1i + γ-8(V177I)	[A, B] -6.05	0.10	890	92.2	3.9	0.968	3
GluA1i + γ-8(G210A)	[A, B] -6.64	0.07	220	98.9	2.3	0.983	3
GluA1i + γ-8(V218T)	[B] -7.80	0.07	15	95.6	1.9	0.982	3
GluA1i + γ-8(V177I / G210A)	[A, B] -5.12	0.12	7600	90.1	7.6	0.969	3
GluA1i + γ-4(I156V/A189G)	[B] -7.59	0.14	25	85.9	3.2	0.933	3
GluA1i + γ-4(A189G)	[A, B] -6.54	0.09	280	88.1	2.7	0.957	5
GluA1i + γ-4(I156V)	[A, B] -6.61	0.09	240	98.8	2.9	0.976	3
GluA1i + γ-4(S140G)	[A] -5.84	0.12	1400	82.0	3.8	0.951	3
GluA1i + γ-4(V138I)	[A] -5.68	0.16	2000	74.5	5.3	0.926	3
GluA1i + γ-2(I153V)	[C, E] -6.20	0.06	620	100.1	2.5	0.987	3
GluA1i + γ-2(A184G)	[C, D] -5.95	0.04	1100	95.2	1.5	0.995	3
GluA1i + γ-2(I153V/A184G)	[C] -6.99	0.08	100	98.0	2.6	0.965	4

The CRCs were fitted with 3-parameter sigmoidal curve fit, and calculated IC_{50} and I_{max}. Post-hoc statistical significance test after ANOVA was carried out for Log[IC_{50}] by Dunnett's test. [A] $p<0.001$ compared to GluA1 + γ-8, [B] $p<0.001$ compared to GluA1 + γ-4, [C] $p<0.001$ compared to GluA1 + γ-2, [D] $p<0.001$ compared to GluA1 + γ-2(I153V/A184G), [E] $p<0.05$ compared to GluA1 + γ-2(I153V/A184G)

Supplementary Table 1f Summary of the pharmacology for the native AMPA receptors in acutely isolated rodent neurons

Rat – LY3130481 Summary

	Log[IC50 (M)]		IC50 (nM)	Imax (%)			
	Mean	SEM		Mean	SEM	R^2	n
Rat Hippocampal	-7.18	0.15	66	72.1	4.6	0.831	7
Rat Cortical	-7.03	0.12	93	59.7	3.1	0.784	14

Mouse – LY3130481 summary

	Log[IC50 (M)]		IC50 (nM)	Imax (%)		nH			
	Mean	SEM		Mean	SEM	Mean	SEM	R^2	n
γ-8$^{+/+}$ Hippocampal	-7.56	0.09	27.0	82.0	2.7	-1.054	0.182	0.848	19
γ-8$^{+/+}$ Cortical	-7.08	0.29	83	55.4	6.3			0.644	5

Rat – Perampanel Summary

	Log[IC50 (M)]		IC50 (nM)	Imax (%)			
	Mean	SEM		Mean	SEM	R^2	n
Rat Hippocampal	-7.27	0.05	53	101.4	1.7	0.984	6
Rat Cortical	-7.30	0.04	49	101.5	1.4	0.989	6
Rat Purkinje	-7.31	0.06	48	101.8	2.3	0.977	5

Values are listed when the R^2 of fitted curves are larger than 0.6. Hill coefficients (nH) were calculated by 4-parameter sigmoidal curve fit, only when we measured more than 12 concentration points. The remaining CRCs were fitted with 3-parameter sigmoidal curve fit. For LY3130481 CRCs, rat Purkinje: n = 5, mouse γ-8$^{-/-}$ Hippocampal: n = 7, γ-8$^{-/-}$ Cortical: n = 7

Table 2 Summary of the radioligand displacement by LY3130481 for various receptors

Receptor	Receptor Source	Radioligand	[Radio-ligand]	Cold competitor	[Cold competitor]	% inhibition of specific binding [LY3130481] 1 µM	% inhibition of specific binding [LY3130481] 10 µM
CB1	human recombinant (CHO cells)	[^{3}H]CP 55940	0.5 nM	WIN 55212-2	10 µM	**1.6**	**18.9**
D_1	human recombinant (CHO cells)	[^{3}H]SCH 23390	0.3 nM	SCH 23390	1 µM	**-0.6**	**6.1**
D_{2S}	human recombinant (HEK293 cells)	[^{3}H]methylspiperone	0.3 nM	(+)butaclamol	10 µM	**5**	**5.6**
$GABA_{A1}$ (α1,β2,γ2)	human recombinant (CHO cells)	[^{3}H]muscimol	15 nM	muscimol	10 µM	**-6.8**	**-8.8**
nAChR (α4β2)	human recombinant (SH-SY5Y cells)	[^{3}H]cytisine	0.6 nM	nicotine	10 µM	**6.2**	**-5.8**
δ2 opioid receptor	human recombinant (CHO cells)	[^{3}H]DADLE	0.5 nM	naltrexone	10 µM	**5.8**	**7.3**
κ opioid receptor	rat recombinant (CHO cells)	[^{3}H]U 69593	1 nM	naloxone	10 µM	**4.9**	**13.3**
µ opioid receptor	human recombinant (HEK293 cells)	[^{3}H]DAMGO	0.5 nM	naloxone	10 µM	**7.9**	**23.8**
5-HT_{2C}	human recombinant (HEK293 cells)	[^{125}I](±)DOI	0.1 nM	(±)DOI	10 µM	**-1.2**	**-5.6**
benzodiazepine receptor	rat cerebral cortex	[^{3}H]flunitrazepam	0.4 nM	diazepam	3 µM	**-16.3**	**9.9**
NMDA	rat cerebral cortex	[^{3}H]CGP 39653	5 nM	L-glutamate	100 µM	**3.1**	**-8.8**
PCP	rat cerebral cortex	[^{3}H]TCP	10 nM	MK 801	10 µM	**-10.3**	**-17.3**
N-type Ca2+ channel	rat cerebral cortex	[^{125}I]ω-conotoxin (GVIA)	0.001 nM	ω-conotoxin (GVIA)	10 nM	**6.8**	**36.5**
K_V channel	rat cerebral cortex	[^{125}I]α-dentrotoxin	0.01 nM	α-dendrotoxin	50 nM	**-16**	**-12.1**
Na^+ channel	rat cerebral cortex	[^{3}H]batrachotoxin	10 nM	veratridine	300 µM	**10.5**	**14.2**
GABA-gated Cl- channels	rat cerebral cortex	[^{35}S]TBPS	3 nM	picrotoxinin	20 µM	**1.9**	**33.7**
norepinephrine transporter	human recombinant (CHO cells)	[^{3}H]nisoxetine	1 nM	desipramine	1 µM	**9.3**	**22.4**
GABA transporter	rat cerebral cortex	[^{3}H]GABA + 10 µM isoguvacine + 10 µM baclofen	10 nM	GABA	1 mM	**1.1**	**2.3**
5-HT transporter	human recombinant (CHO cells)	[^{3}H]imipramine	2 nM	imipramine	10 µM	**9.3**	**50**

LY3130481 did not affect the radioligand binding to the receptors / transporters shown above. The summary of the selectivity assay by radioligand displacement Specific radioligand binding was assessed as described in Method section. The combinations of receptor / transporters and radioligands, and cold competitors to determine the specific binding were listed. Percent inhibition of the specific binding of the radioligands to the corresponding receptors by 1 or 10 µM LY3130481 are shown in the right column.

Table 3a The LY3130481 effects on kainate and NMDA receptors

Receptor	Potentiator (EC50)	Antagonist (IC50)
GluK2	ND	>10,000
GluN1 / GluN2A	>10,000	>6,670
GluN1 / GluN2B	>10,000	>6,670

ND: not determined

LY3130481 did not have either potentiator or antagonist activities to kainate or NMDA receptor. The EC50 as a potentiator and IC50 as an antagonist were determined by FLIPR as described in Method / FLIPR screening section.

Table 3b The LY3130481 effects on metabotropic glutamate receptors

Receptor	Potentiation %	[LY3130481] (μM)	Inhibition %	[LY3130481] (μM)
mGluR1	19.1	12.5	-0.6	12.5
mGluR2	10.3	12.5	-3.5	12.5
mGluR3	14.8	12.5	3.4	12.5
mGluR4	2.1	12.5	6	12.5
mGluR5	-0.9	25	-8.25	12.5
mGluR8	12.8	12.5	15.7	12.5

LY3130481 did not affect mGluR functions. All mGluR functions were determined by intracellular calcium mobilization by FLIPR as described in Method / FLIPR screening section. Gi-coupled mGluRs were co-transfected with promiscuous Gα, Gα15 cDNA to translate the mGluR activation to calcium mobilization. The percentages of potentiation and inhibition in the presence of LY3130481 at the indicated concentrations are shown.

Figure 1

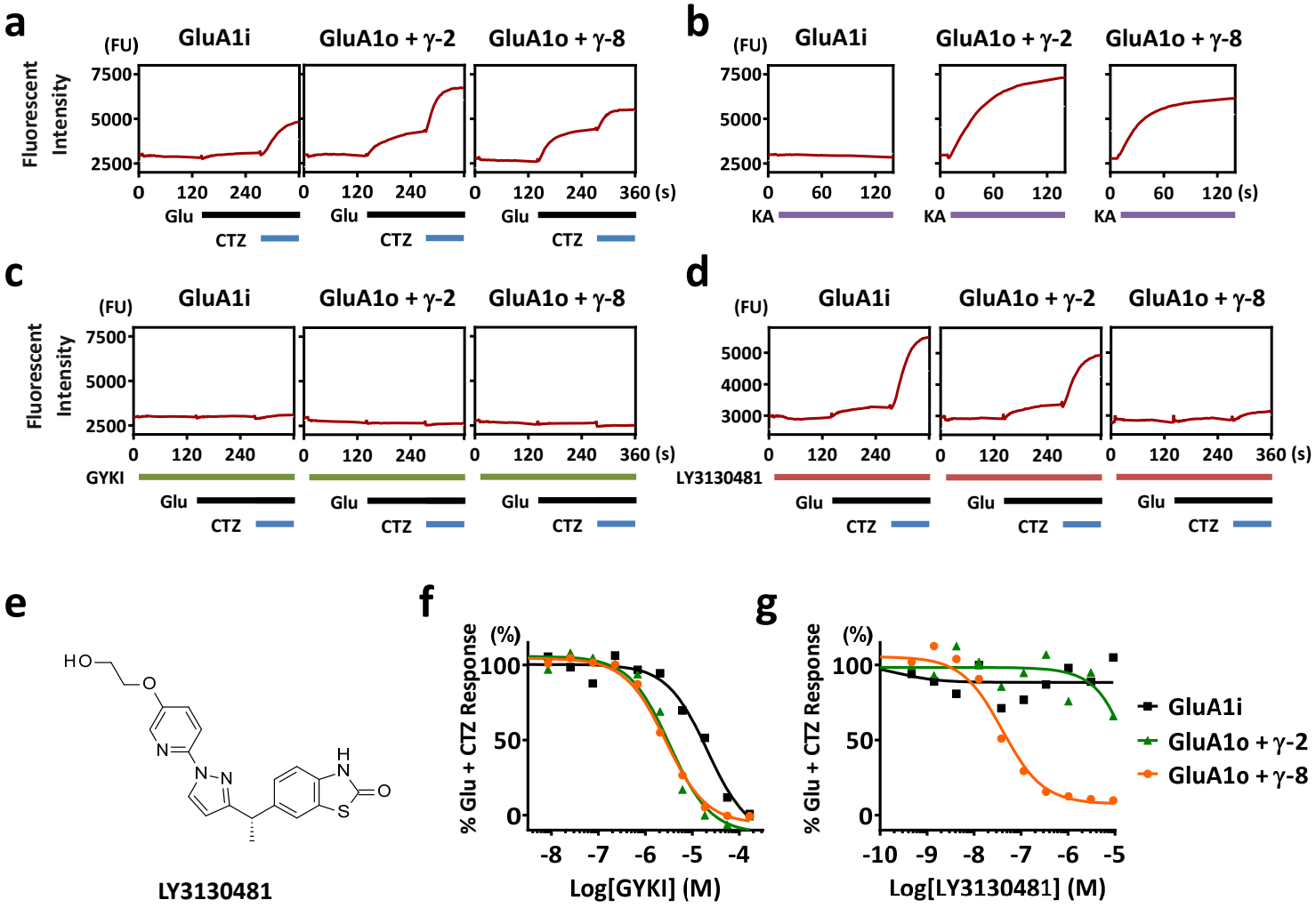
a
GluA1i
GluA1o + γ-2
GluA1o + γ-8
(FU)
Fluorescent Intensity
7500
5000
2500
0 120 240 0 120 240 0 120 240 360 (s)
Glu
CTZ
b
GluA1i
GluA1o + γ-2
GluA1o + γ-8
(FU)
7500
5000
2500
0 60 120 0 60 120 0 60 120 (s)
KA
c
GluA1i
GluA1o + γ-2
GluA1o + γ-8
(FU)
Fluorescent Intensity
7500
5000
2500
0 120 240 0 120 240 0 120 240 360 (s)
GYKI
Glu
CTZ
d
GluA1i
GluA1o + γ-2
GluA1o + γ-8
(FU)
5000
4000
3000
0 120 240 0 120 240 0 120 240 360 (s)
LY3130481
Glu
CTZ
e
HO
O
N
N
N
H
N
O
S
LY3130481
f
% Glu + CTZ Response
(%)
100
50
0
-8 -7 -6 -5 -4
Log[GYKI] (M)
g
% Glu + CTZ Response
(%)
100
50
0
-10 -9 -8 -7 -6 -5
Log[LY3130481] (M)
GluA1i
GluA1o + γ-2
GluA1o + γ-8

Figure 2

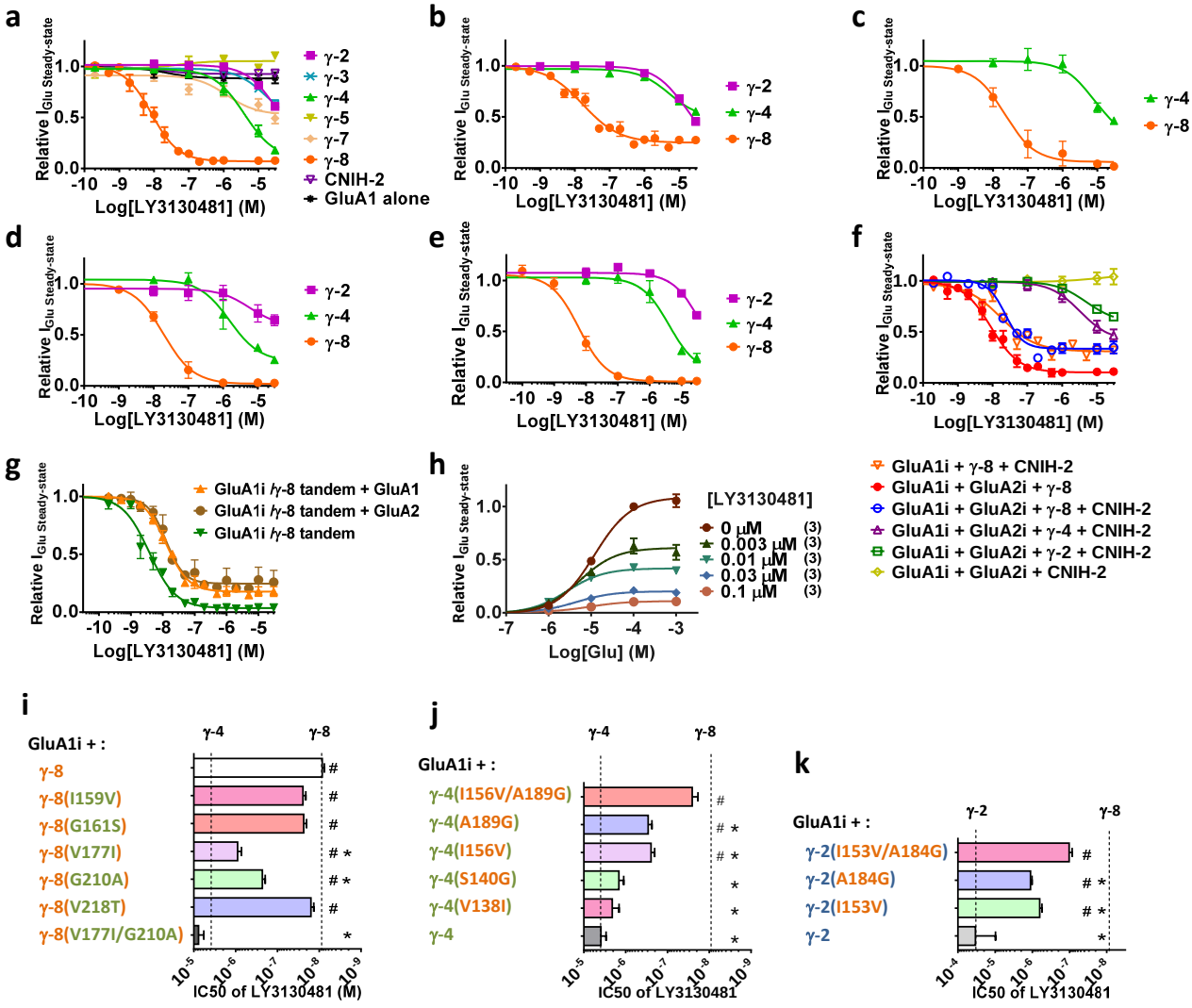
a
b
c
d
e
f
g
h
i
j
k
Relative IGlu Steady-state
Log[LY3130481] (M)
γ-2
γ-3
γ-4
γ-5
γ-7
γ-8
CNIH-2
GluA1 alone
GluA1i /γ-8 tandem + GluA1
GluA1i /γ-8 tandem + GluA2
GluA1i /γ-8 tandem
[LY3130481]
0 μM (3)
0.003 μM (3)
0.01 μM (3)
0.03 μM (3)
0.1 μM (3)
Log[Glu] (M)
GluA1i + γ-8 + CNIH-2
GluA1i + GluA2i + γ-8
GluA1i + GluA2i + γ-8 + CNIH-2
GluA1i + GluA2i + γ-4 + CNIH-2
GluA1i + GluA2i + γ-2 + CNIH-2
GluA1i + GluA2i + CNIH-2
GluA1i + :
γ-8
γ-8(I159V)
γ-8(G161S)
γ-8(V177I)
γ-8(G210A)
γ-8(V218T)
γ-8(V177I/G210A)
IC50 of LY3130481 (M)
γ-4(I156V/A189G)
γ-4(A189G)
γ-4(I156V)
γ-4(S140G)
γ-4(V138I)
γ-4
γ-2(I153V/A184G)
γ-2(A184G)
γ-2(I153V)
γ-2

Figure 3

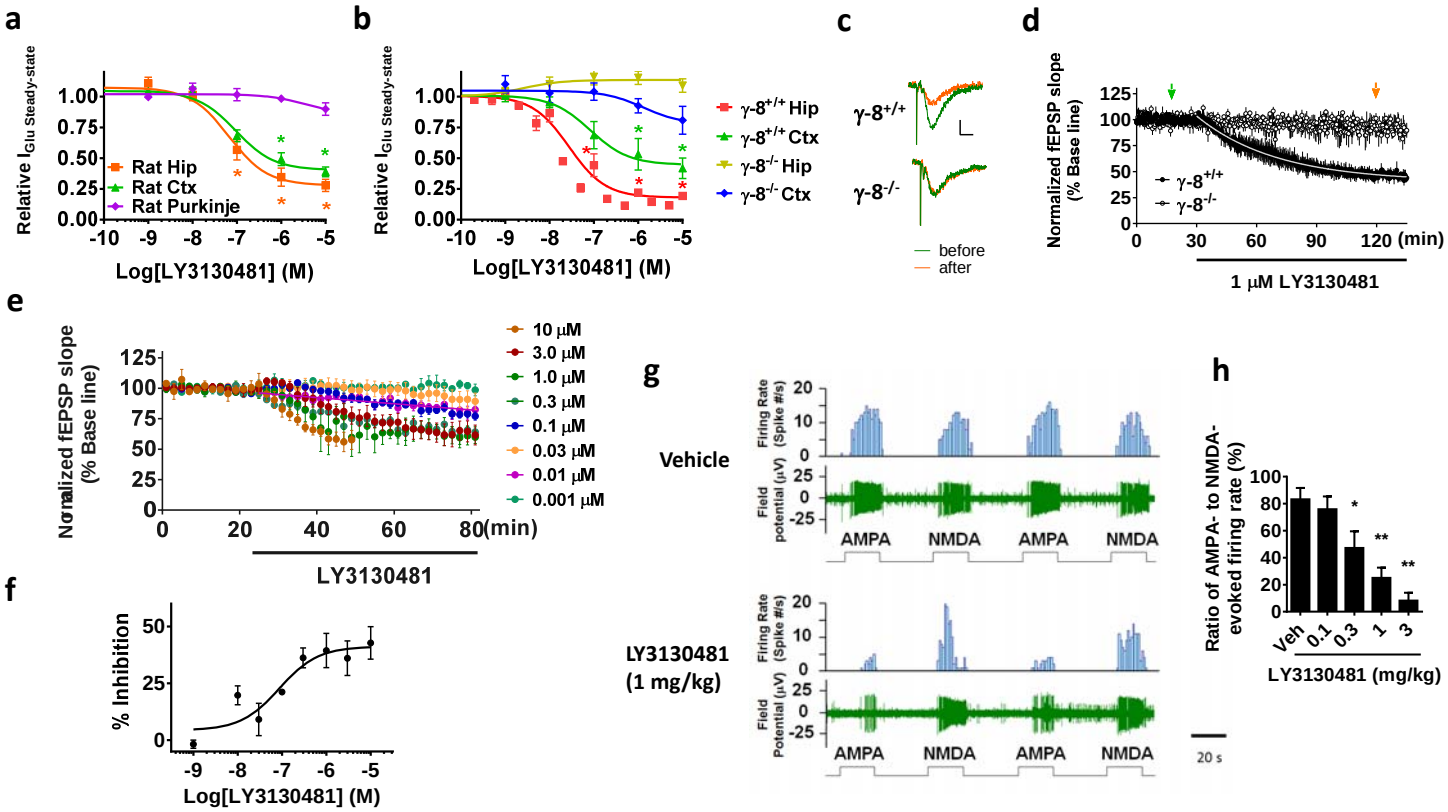
a
Relative $I_{Glu\ Steady\text{-}state}$
Rat Hip
Rat Ctx
Rat Purkinje
Log[LY3130481] (M)
b
Relative $I_{Glu\ Steady\text{-}state}$
γ-8+/+ Hip
γ-8+/+ Ctx
γ-8-/- Hip
γ-8-/- Ctx
Log[LY3130481] (M)
c
γ-8+/+
γ-8-/-
before
after
d
Normalized fEPSP slope (% Base line)
γ-8+/+
γ-8-/-
1 μM LY3130481
e
Normalized fEPSP slope (% Base line)
10 μM
3.0 μM
1.0 μM
0.3 μM
0.1 μM
0.03 μM
0.01 μM
0.001 μM
LY3130481
f
% Inhibition
Log[LY3130481] (M)
g
Vehicle
LY3130481 (1 mg/kg)
Firing Rate (Spike #/s)
Field potential (μV)
AMPA
NMDA
20 s
h
Ratio of AMPA- to NMDA-evoked firing rate (%)
Veh
LY3130481 (mg/kg)

Figure 4

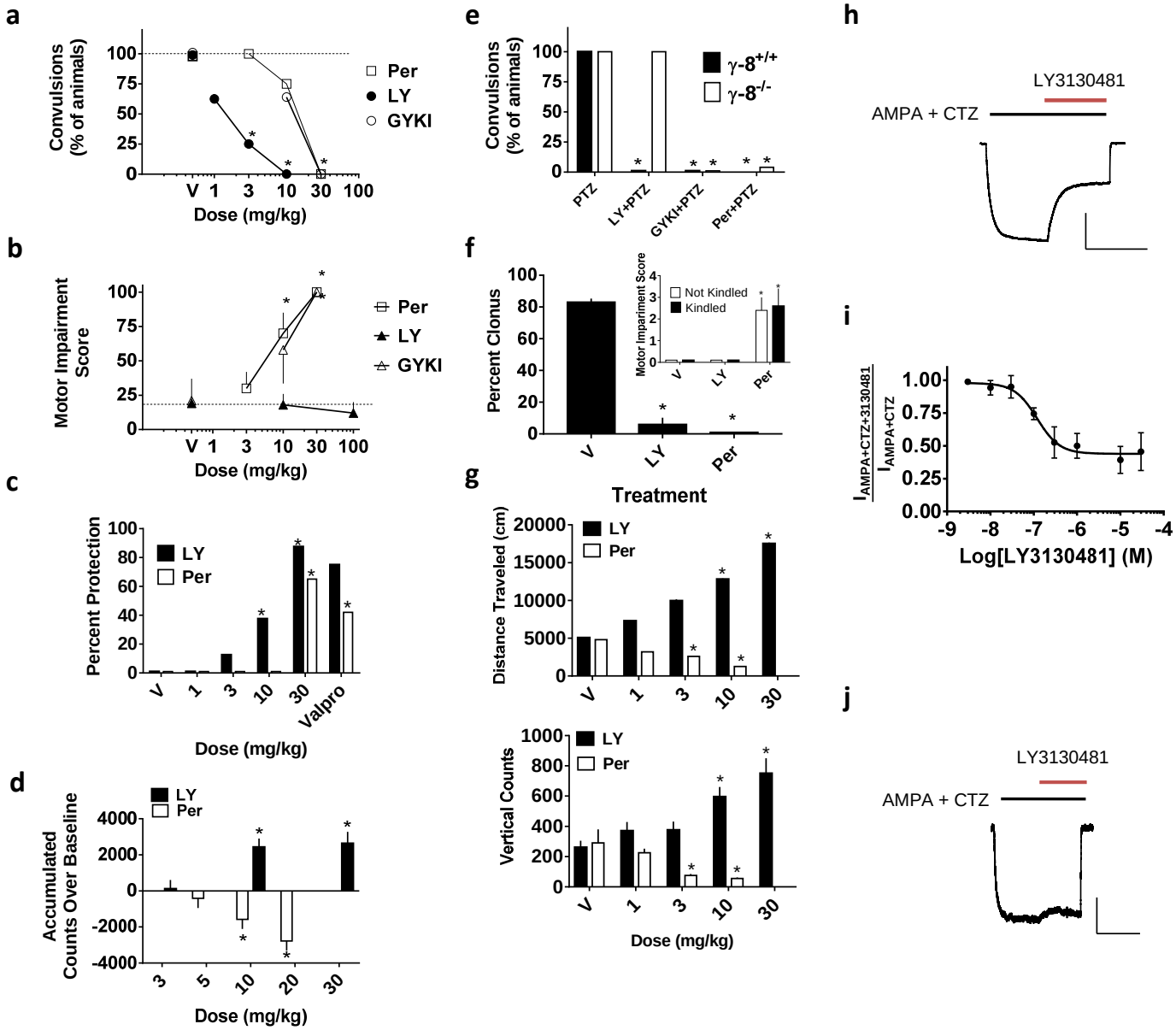
a
Convulsions (% of animals)
100
75
50
25
0
V 1 3 10 30 100
Dose (mg/kg)
Per
LY
GYKI
b
Motor Impairment Score
100
75
50
25
0
V 1 3 10 30 100
Dose (mg/kg)
Per
LY
GYKI
c
Percent Protection
100
80
60
40
20
0
LY
Per
V 1 3 10 30 Valpro
Dose (mg/kg)
d
Accumulated Counts Over Baseline
4000
2000
0
-2000
-4000
LY
Per
3 5 10 20 30
Dose (mg/kg)
e
Convulsions (% of animals)
100
75
50
25
0
γ-8+/+
γ-8-/-
PTZ
LY+PTZ
GYKI+PTZ
Per+PTZ
f
Percent Clonus
100
80
60
40
20
0
V
LY
Per
Treatment
Motor Impairment Score
4
3
2
1
0
Not Kindled
Kindled
V
LY
Per
g
Distance Traveled (cm)
20000
15000
10000
5000
0
LY
Per
V 1 3 10 30
Vertical Counts
1000
800
600
400
200
0
LY
Per
V 1 3 10 30
Dose (mg/kg)
h
LY3130481
AMPA + CTZ
i
I AMPA+CTZ+3130481 / I AMPA+CTZ
1.00
0.75
0.50
0.25
0.00
-9 -8 -7 -6 -5 -4
Log[LY3130481] (M)
j
LY3130481
AMPA + CTZ

Supplementary Figure 1

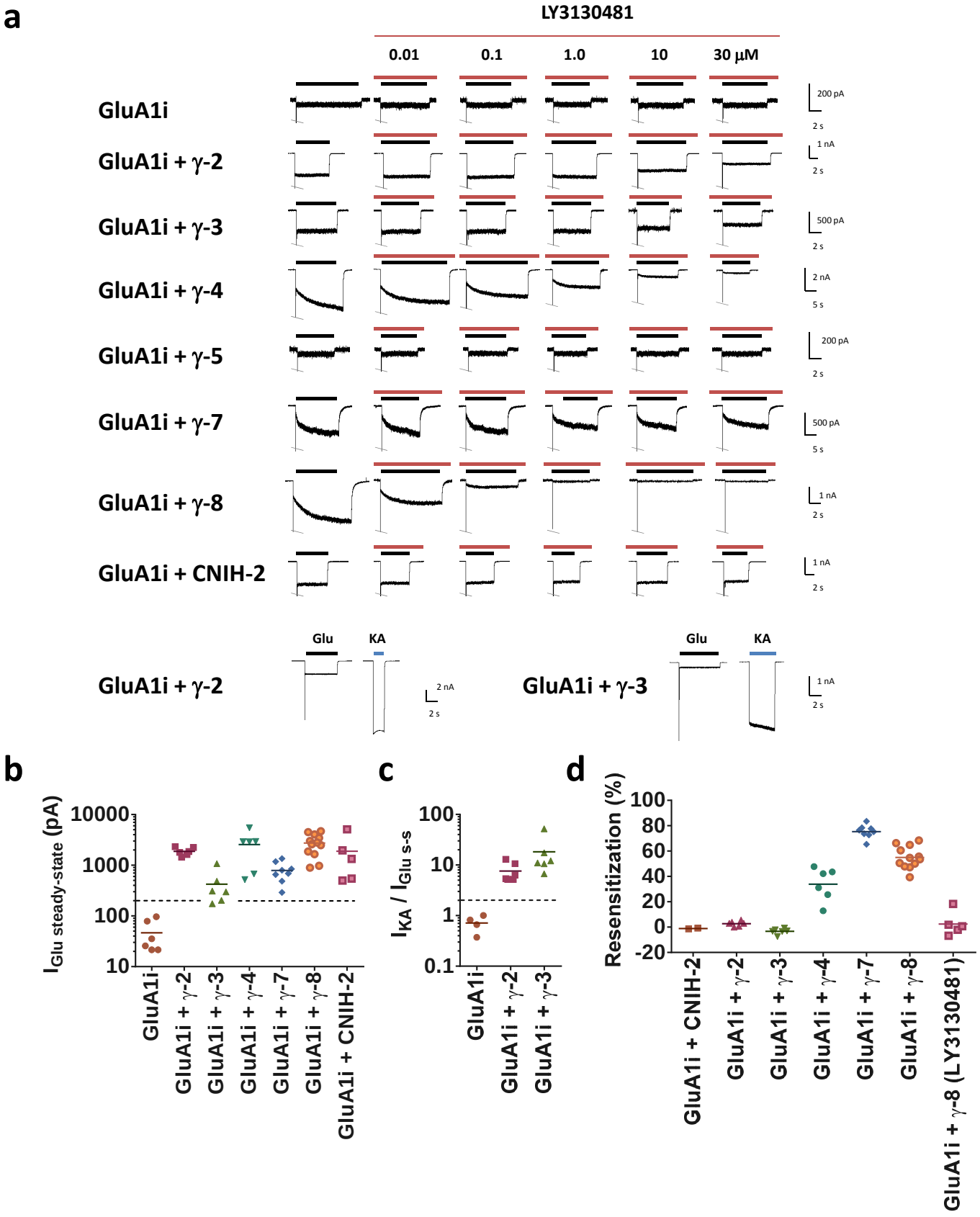

Supplementary Figure 2

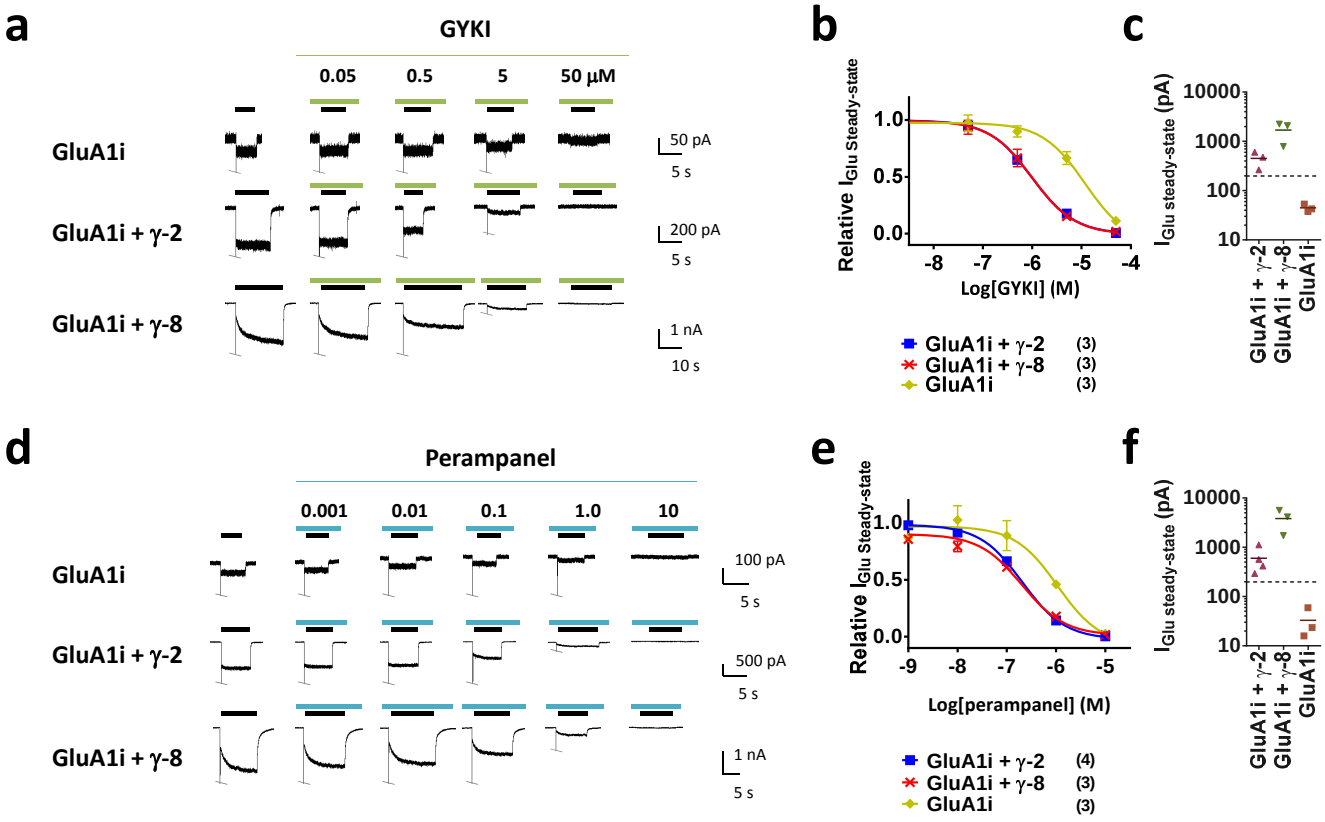

Supplementary Figure 3

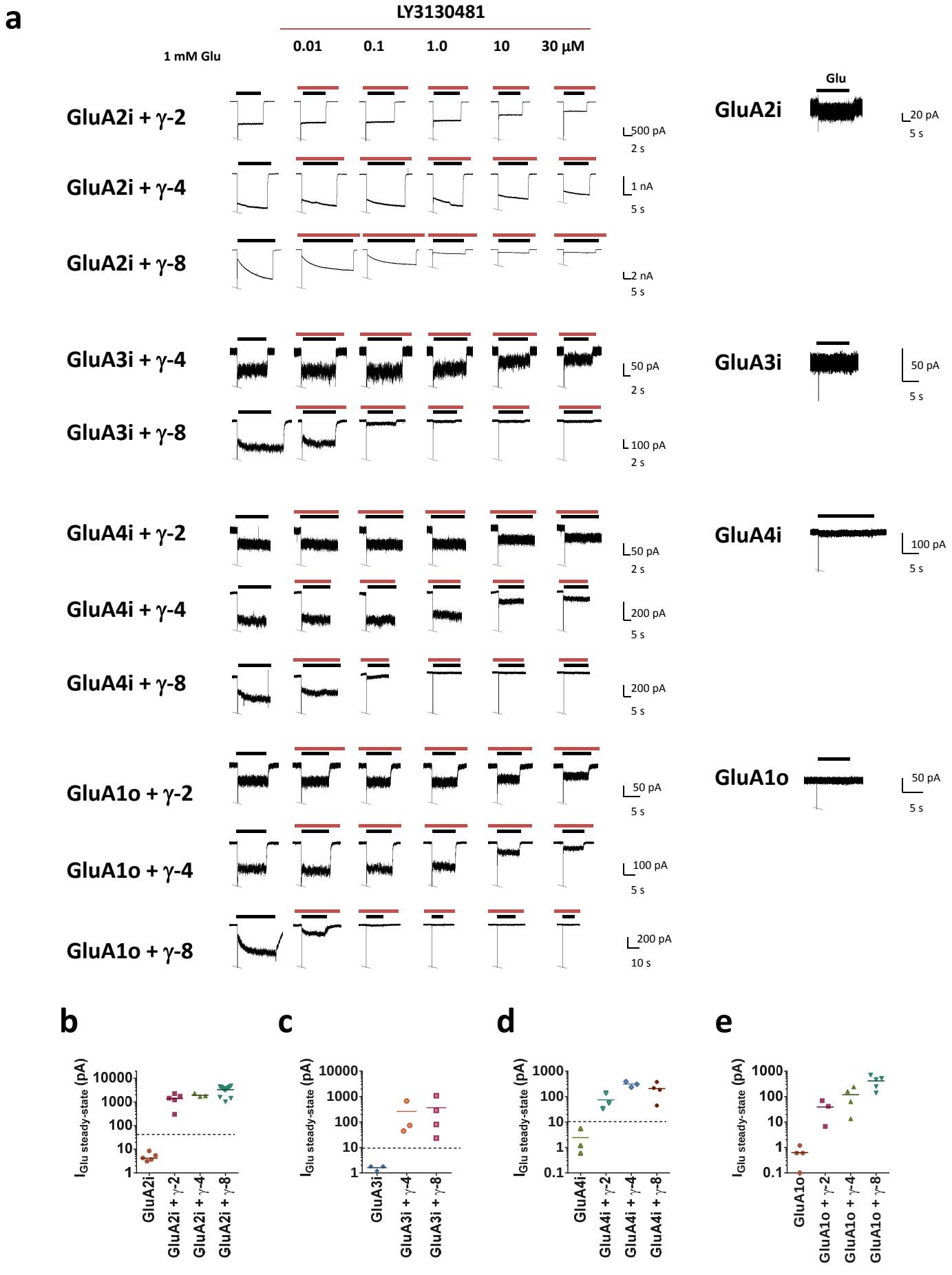

Supplementary Figure 4

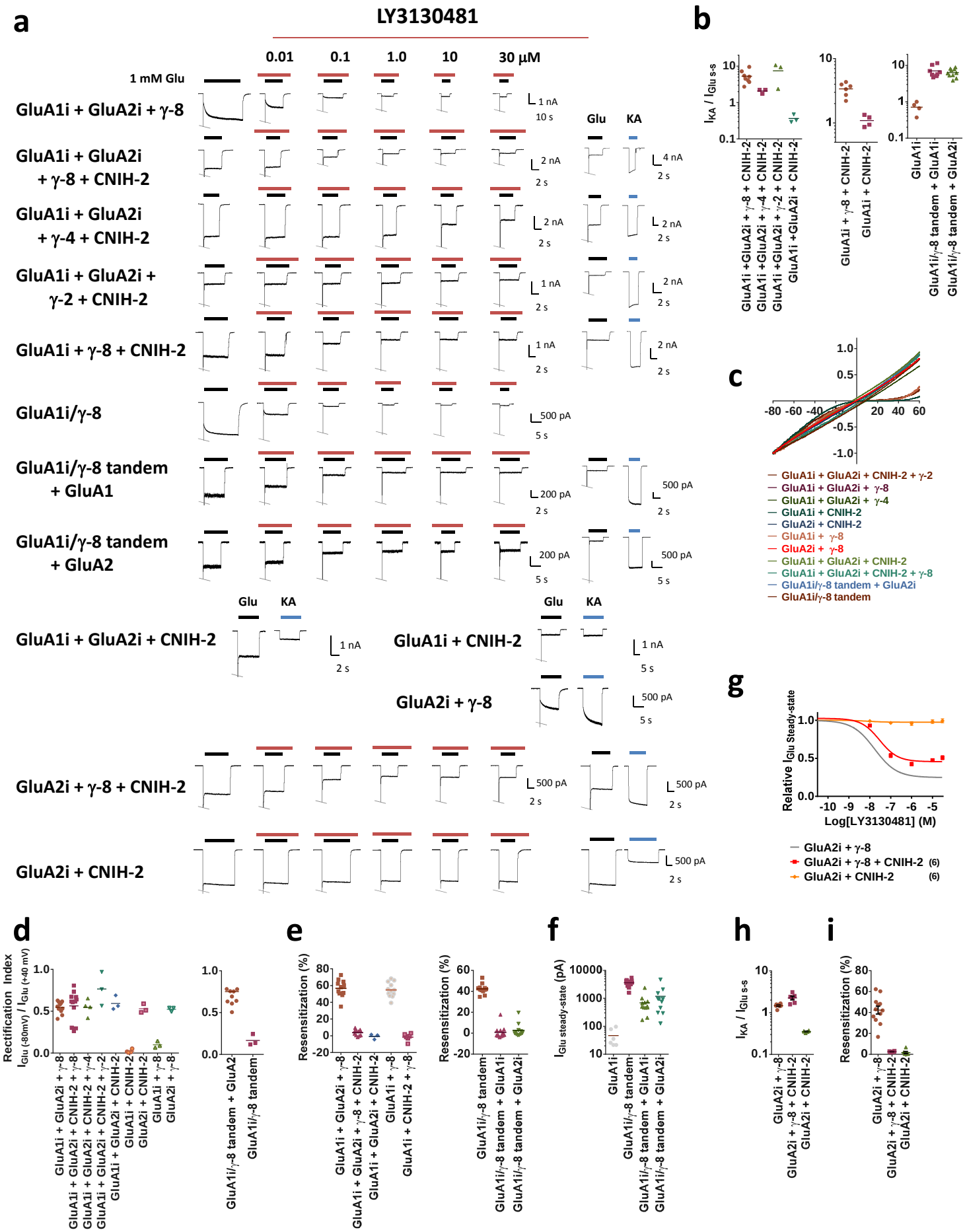

Supplementary Figure 5

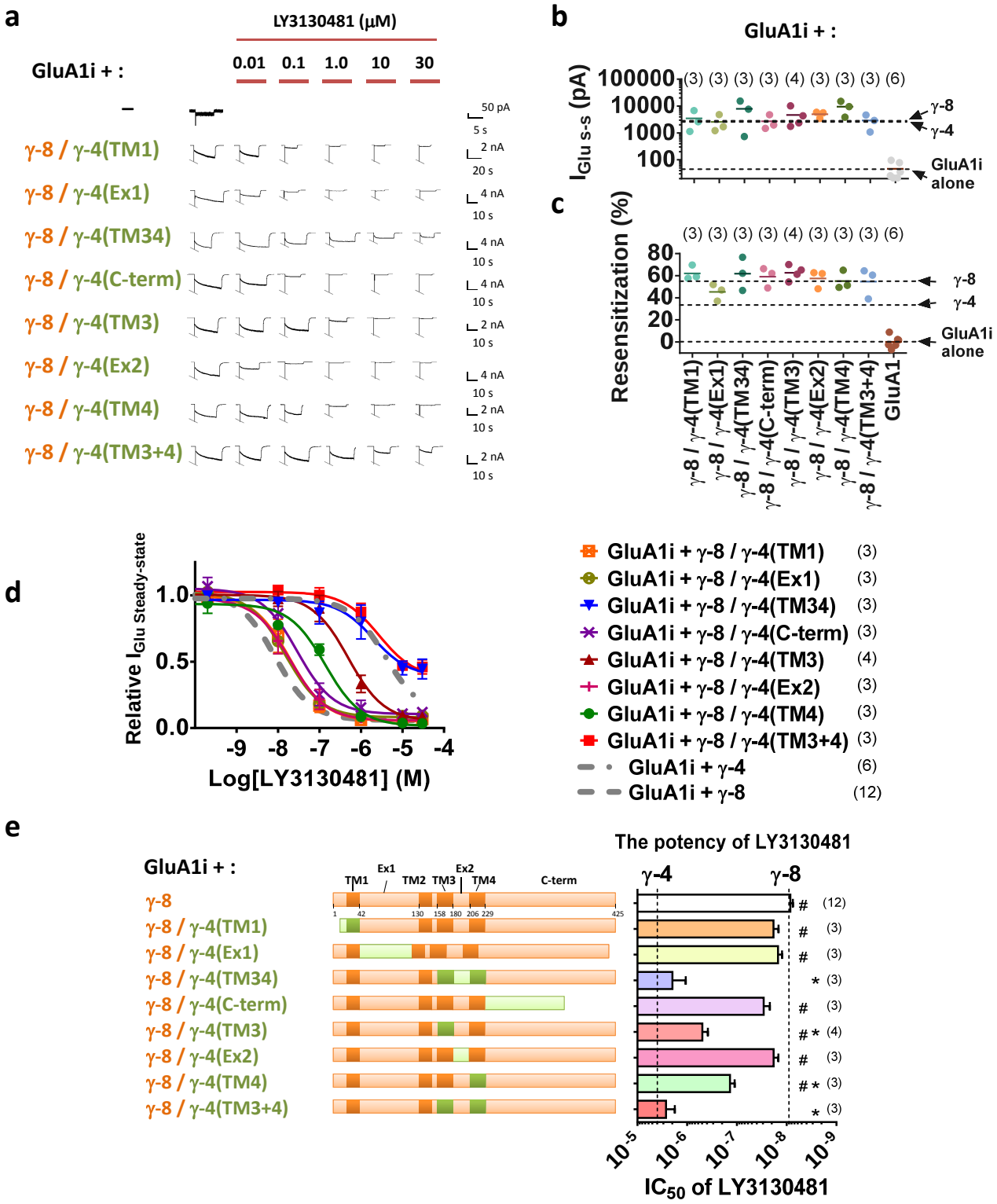

Supplementary Figure 6

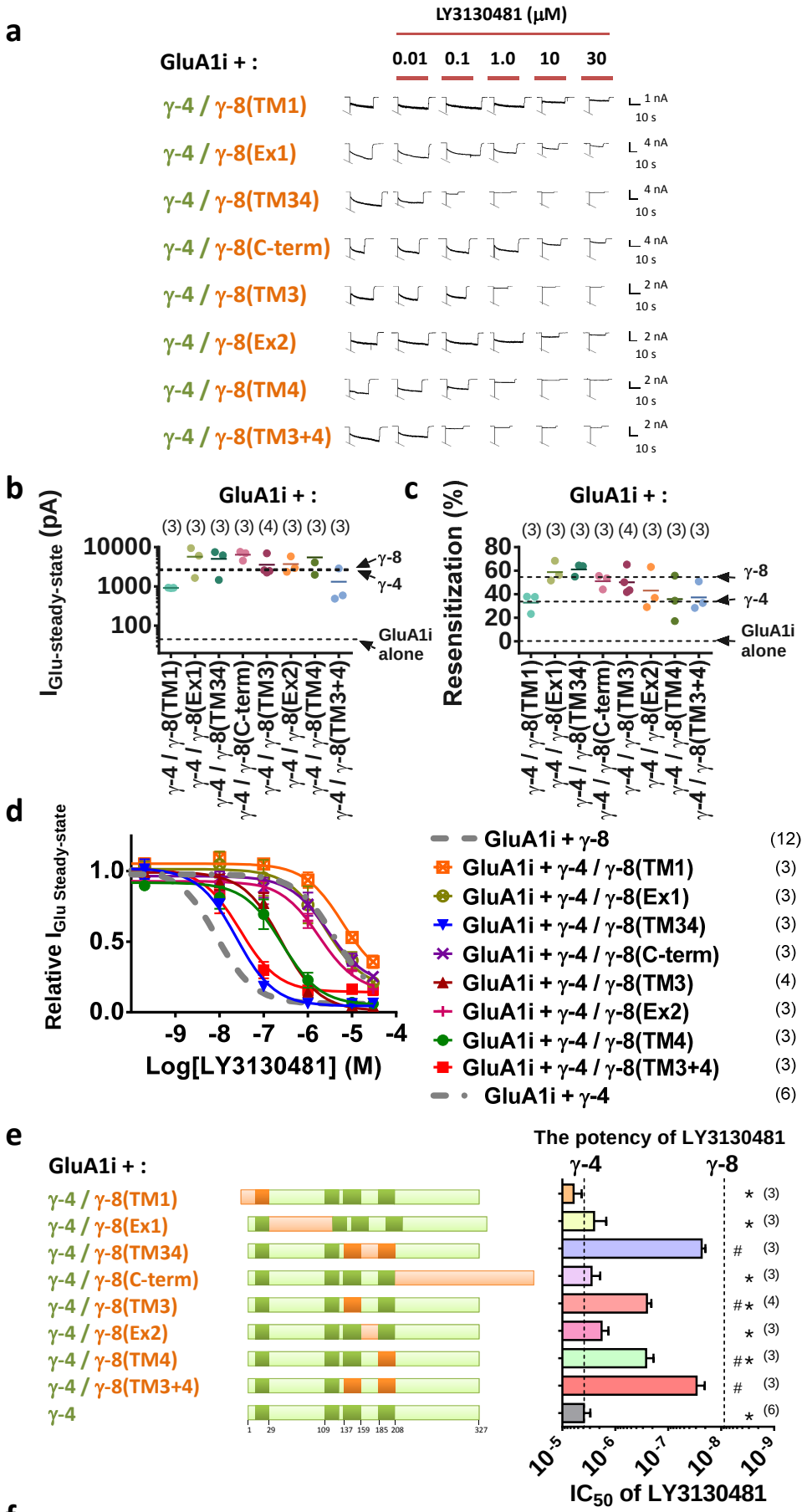

Supplementary Figure 7

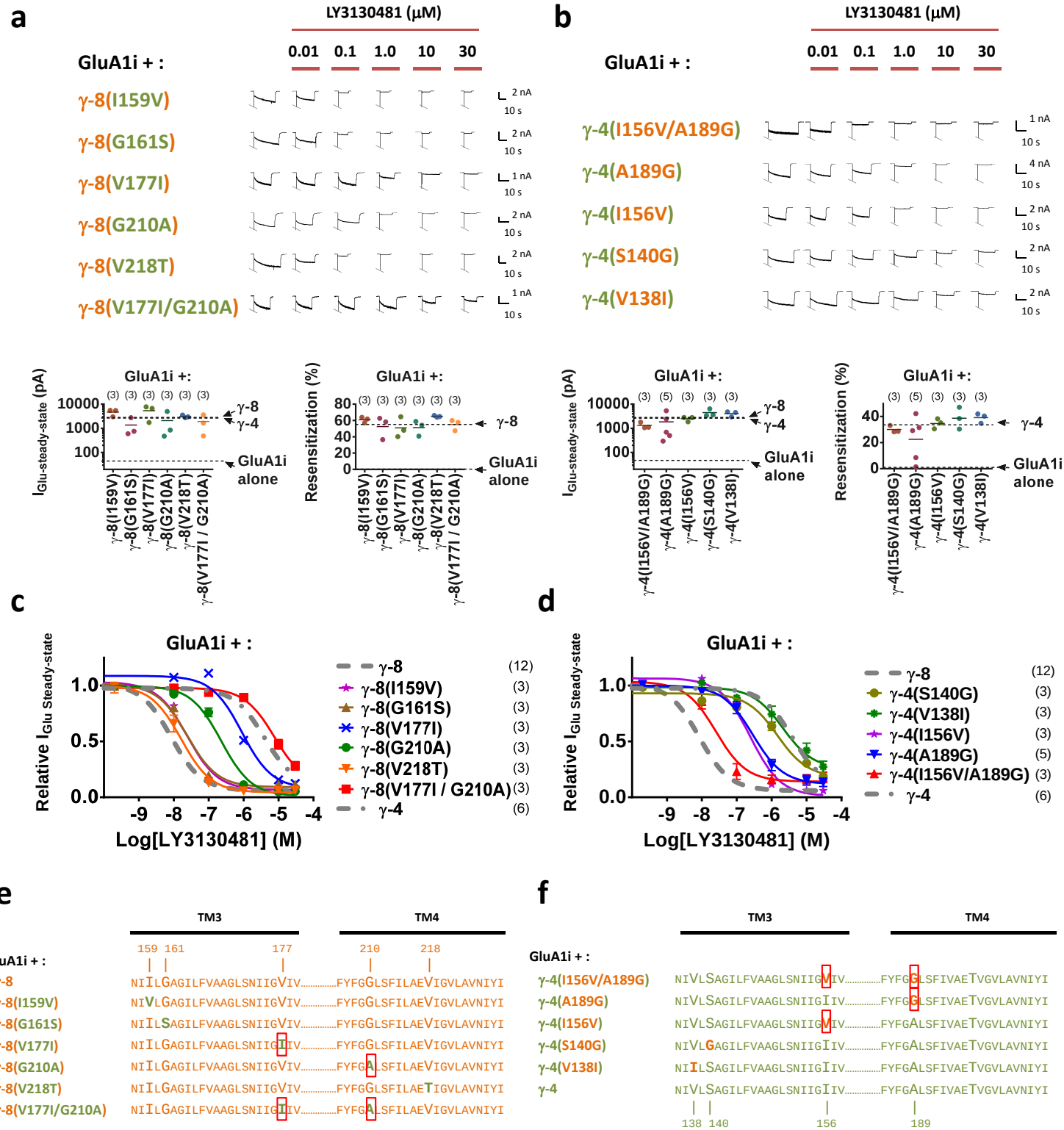

Supplementary Figure 8

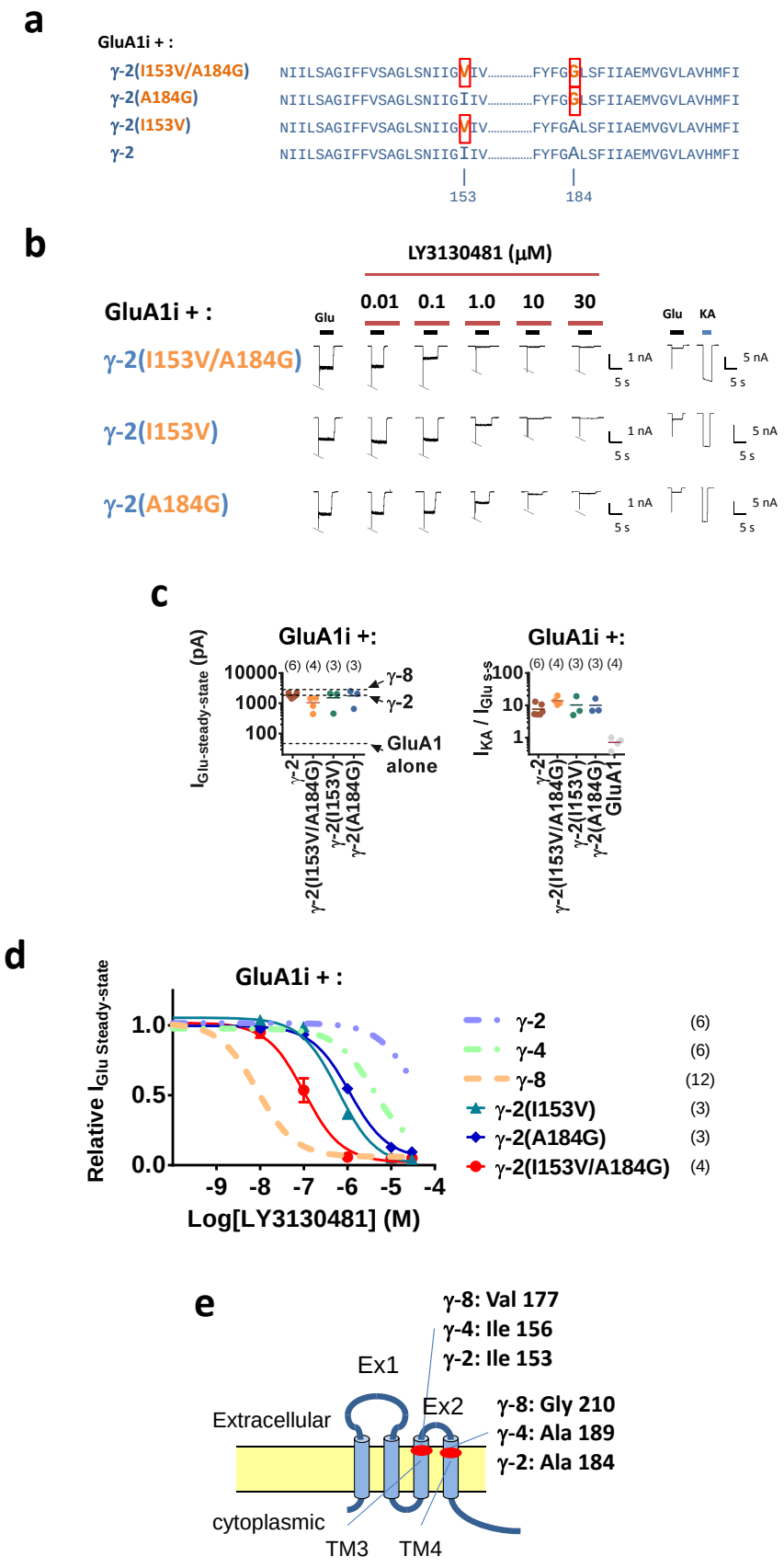

Supplementary Figure 9

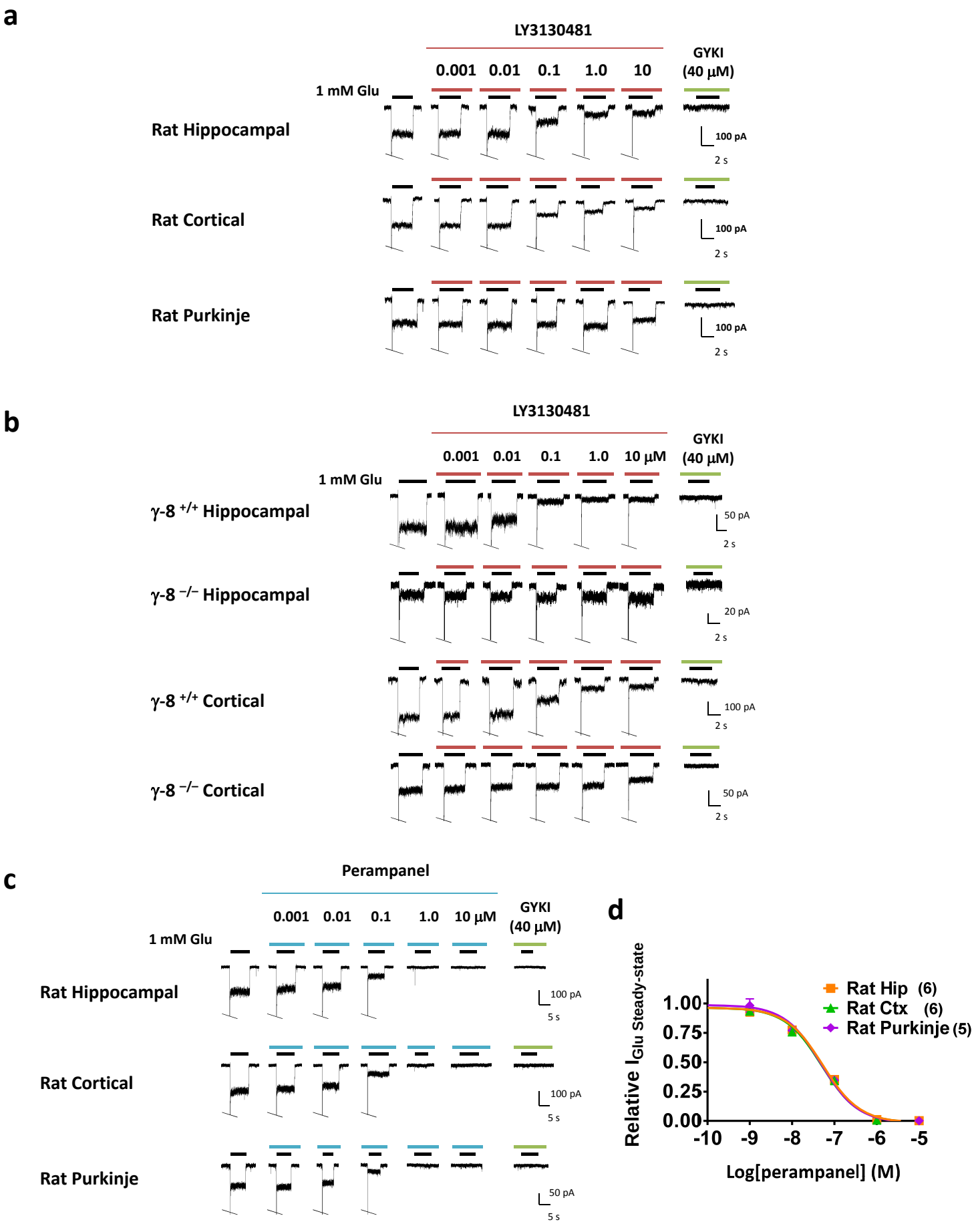

Supplementary Figure 10

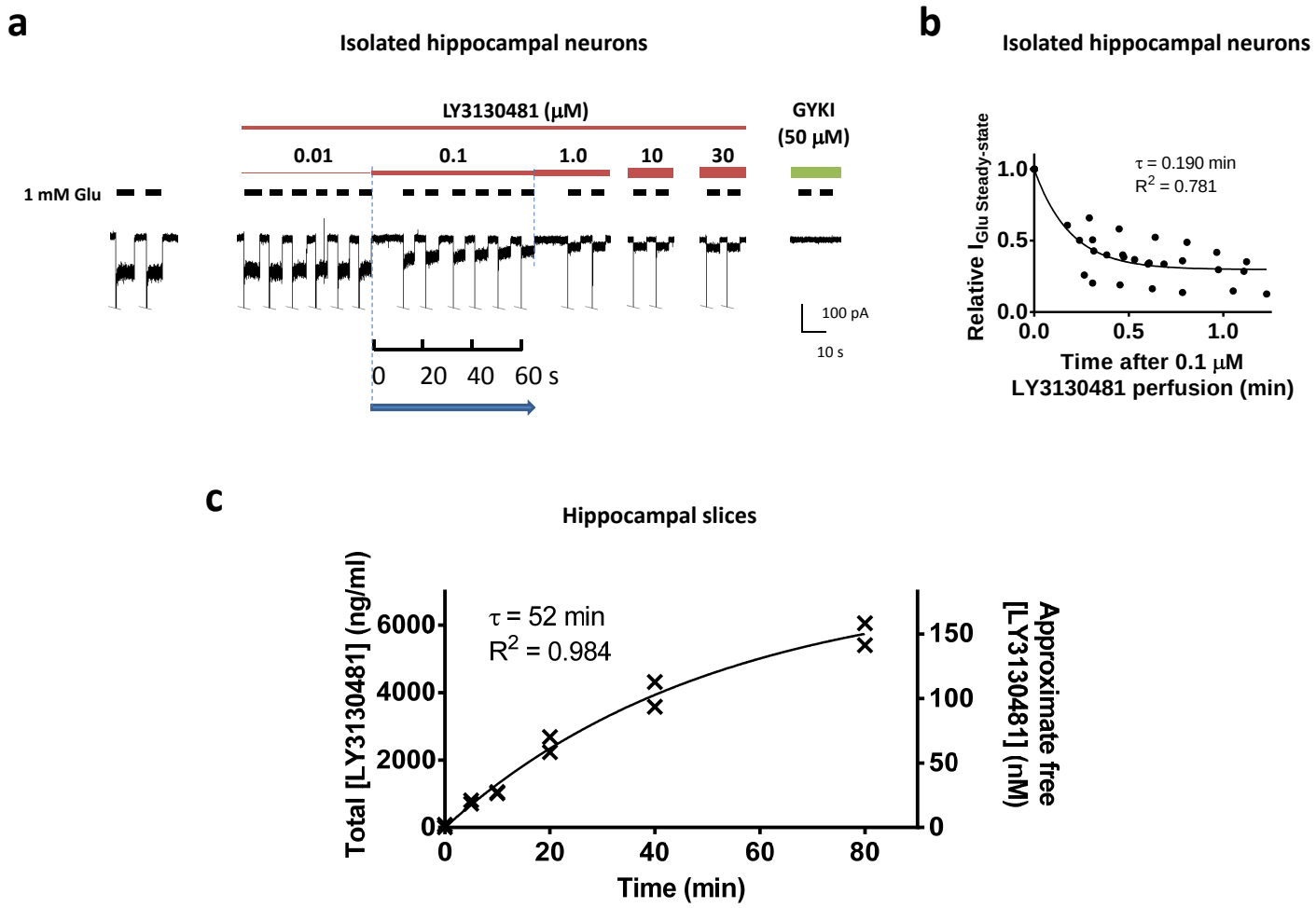

Supplementary Figure 11

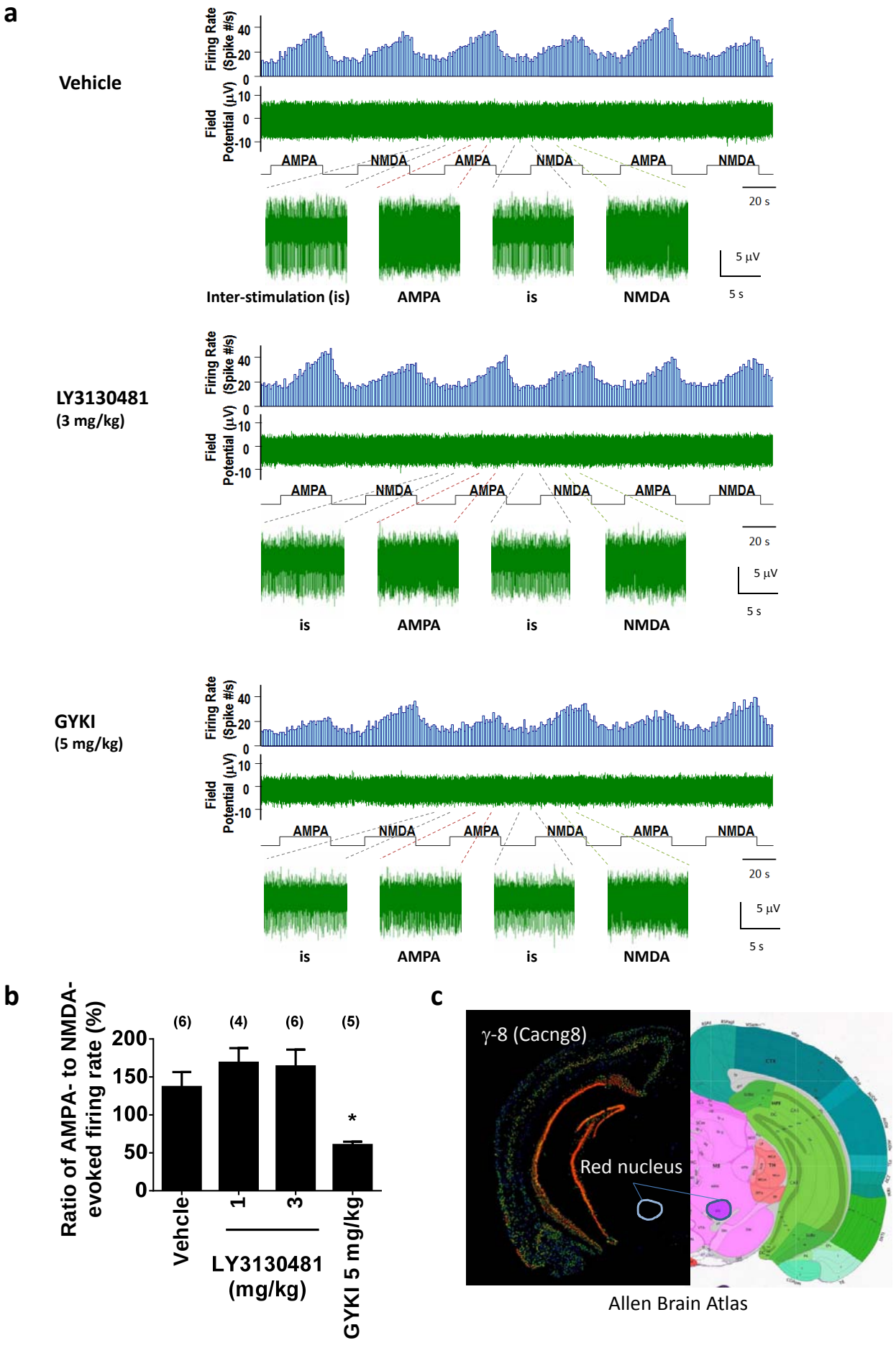

Supplementary Figure 12